



## HHS PUBLIC ACCESS

Author manuscript

Pain. Author manuscript; available in PMC 2019 May 01.

Published in final edited form as:

Pain. 2018 May ; 159(5): 849–863. doi:10.1097/j.pain.0000000000001152.

## Disruption of nNOS-NOS1AP protein-protein interactions suppresses neuropathic pain in mice

Wan-Hung Lee<sup>1</sup>, Li-Li Li<sup>2</sup>, Aarti Chawla<sup>3</sup>, Andy Hudmon<sup>3</sup>, Yvonne Y. Lai<sup>4</sup>, Michael J. Courtney<sup>2</sup>, and Andrea G. Hohmann<sup>1,4,5,\*</sup>

<sup>1</sup>Biochemistry Interdisciplinary Graduate Program, Molecular and Cellular Biochemistry Department, Indiana University, Bloomington, IN <sup>2</sup>Turku Centre for Biotechnology, University of Turku and Åbo Academy University, Turku, Finland <sup>3</sup>Department of Biochemistry and Molecular Biology, Indiana University School of Medicine, Indianapolis, IN <sup>4</sup>Department of Psychological and Brain Sciences, Indiana University, Bloomington, IN <sup>5</sup>Gill Center for Biomolecular Science, Bloomington, IN

### Abstract

Elevated *N*-methyl-D-aspartate receptor (NMDAR) activity is linked to central sensitization and chronic pain. However, NMDAR antagonists display limited therapeutic potential due to their adverse side effects. Novel approaches targeting the NR2B-PSD95-nNOS complex to disrupt signaling pathways downstream of NMDARs show efficacy in preclinical pain models. Here, we evaluated the involvement of interactions between neuronal nitric oxide synthase (nNOS) and the nitric oxide synthase 1 adaptor protein (NOS1AP) in pronociceptive signaling and neuropathic pain. TAT-GESV, a peptide inhibitor of the nNOS-NOS1AP complex, disrupted the *in vitro* binding between nNOS and its downstream protein partner NOS1AP but not its upstream protein partner postsynaptic density 95 kDa (PSD95). Putative inactive peptides (TAT-cp4GESV, TAT-GESV 1) failed to do so. Only the active peptide protected primary cortical neurons from glutamate/glycine-induced excitotoxicity. TAT-GESV, administered intrathecally (i.t.), suppressed mechanical and cold allodynia induced by either the chemotherapeutic agent paclitaxel or a traumatic nerve injury induced by partial sciatic nerve ligation (PSNL). TAT-GESV also blocked the paclitaxel-induced phosphorylation at Ser15 of p53, a substrate of p38 MAPK. Finally, TAT-GESV (i.t.) did not induce NMDAR-mediated motor ataxia in the rota-rod test and did not alter basal nociceptive thresholds in the radiant heat tail-flick test. These observations support the hypothesis that anti-allodynic efficacy of an nNOS-NOS1AP disruptor may result, at least in part, from blockade of p38 MAPK-mediated downstream effects. Our studies demonstrate, for the first time, that disrupting nNOS-NOS1AP protein-protein interactions attenuates mechanistically distinct forms of neuropathic pain without unwanted motor ataxic effects of NMDAR antagonists.

\*Address for correspondence: Andrea G. Hohmann, Department of Psychological and Brain Sciences, Indiana University, 1101 E 10<sup>th</sup> Street, Bloomington, IN 47405-7007, USA. Phone: +1 8128560672, hohmanna@indiana.edu.

**Conflict of interest:** YYL is partially employed at Anagin, LLC. The remaining authors (W-HL, L-LI, AC, MJC and AGH) have no conflicts of interest to declare.

## Keywords

Allodynia; Hyperalgesia; Neuropathic pain; NMDA receptor; Neuronal nitric oxide synthase; Nitric oxide synthase 1 adaptor protein

---

## 1. Introduction

Excessive *N*-methyl-D-aspartate receptor (NMDAR) activity is important for central sensitization and development and maintenance of chronic pain. However, NMDAR antagonists have limited therapeutic value due to incomplete efficacy and unwanted side effects [36; 55]. An alternative approach is to disrupt protein-protein interactions downstream of NMDARs that mediate signaling cascades critical for central sensitization. Protein-protein interactions between the NR2B subunit of NMDAR, the scaffolding protein postsynaptic density 95 kDa (PSD95) and the enzyme neuronal nitric oxide synthase (nNOS), referred to as the NR2B-PSD95-nNOS interface, are involved in neuropathological conditions including stroke/ischemia, pain and depression. We and others showed that disrupting PSD95-nNOS [8; 17; 27] and NR2B-PSD95 [13] interactions suppresses pain at doses that lack adverse side effects in rodents [44].

In addition to PSD95, nNOS interacts with nitric oxide synthase 1 adaptor protein (NOS1AP), also known as Carboxy-terminal PDZ ligand of nNOS (CAPON) [24]. Binding of nNOS to NOS1AP occurs through a class III PDZ-PDZ interaction between the canonical PDZ (postsynaptic density 95, PSD95; discs large, Dlg; zonula occludens-1, ZO-1) of nNOS (amino acid (a.a.) 11–98) and both the stabilizing C-terminal tail and indispensable internal ExF motif (a.a. 429–431) of NOS1AP [24; 28; 30; 48]. Interactions between nNOS and NOS1AP are implicated in neuropathological conditions including stroke, anxiety and schizophrenia, and disrupting these interactions is neuroprotective [6; 9; 29; 49; 57]. NMDAR-dependent association of nNOS-NOS1AP activates p38 mitogen-activated protein kinase (p38 MAPK) by recruiting mitogen-activated protein kinase kinase 3 (MKK3) to the complex [15; 29; 38]. Activation of p38 MAPK is observed in preclinical pain models, suggesting that inhibiting p38 MAPK activation may interrupt pronociceptive signaling [11; 25; 26; 31; 58]. Downstream p38 MAPK substrates (e.g. tumor protein p53 (p53)) may underlie cytotoxic and inflammatory effects associated with p38MAPK-activation [65]. However, whether nNOS-NOS1AP interactions are involved in pronociceptive signaling and pathological pain is unknown.

To investigate involvement of nNOS-NOS1AP in pathological pain, we used TAT-GESV, a peptide inhibitor of the consensus binding sequence for the core PDZ domain of nNOS [29; 40]. TAT-GESV attenuates NMDAR-induced cytotoxicity and is neuroprotective in an ischemia model [29; 40]. We evaluated the potency and specificity of TAT-GESV, in comparison to putative inactive peptides (TAT-cp4GESV, TAT-GESV 1), in disrupting nNOS-NOS1AP interactions using AlphaScreen binding assays. The ability of TAT-GESV to disrupt PSD95-nNOS binding was evaluated to assess selectivity. We also verified that TAT-GESV suppresses glutamate/glycine-induced excitotoxicity in primary cortical neurons. Based upon the known critical roles of the peptide ligand terminal valine in target

recognition, we predicted that terminal valine deletion (using TAT-GESV<sub>1</sub>) would prevent the otherwise active peptide from both disrupting nNOS-NOS1AP binding and suppressing neuropathic pain. We tested the hypothesis that intrathecal (i.t.) TAT-GESV, but not TAT-GESV<sub>1</sub>, would suppress mechanical and cold hypersensitivity in mechanistically distinct models of neuropathic pain and investigated potential mechanisms underlying efficacy of nNOS-NOS1AP disruption in lumbar spinal cord of paclitaxel-treated mice. Lastly, we evaluated whether nNOS-NOS1AP disruption lacked unwanted side effects of NMDAR antagonists.

## 2. Materials and methods

### 2.1 Drugs and chemicals

Peptides were obtained from the laboratory of Dr. Michael Courtney (Turku Centre for Biotechnology, University of Turku and Åbo Academy University, Finland) or purchased from GenicBio (Shanghai, China), GeneCust (Dudelange, Luxembourg) or Peptide 2.0 (Chantilly, VA) with at least 95% purity: L-TAT (GRKKRRQRRR); L-TAT-GESV (GRKKRRQRRRYAGQWGESV); L-TAT-GESV<sub>1</sub> (GRKKRRQRRRYAGQWGES): lacking the last C-terminal Val residue; L-TAT-cp4GESV (GRKKRRQRRRGESVYAGQW): the C-terminal GESV tetrapeptide was placed between the TAT sequence and the N-terminal YAGQW pentapeptide. All peptides were dissolved in PBS for AlphaScreen and cell death assays and dissolved in saline (Aquilite System; Hospira, Inc, Lake Forest, IL) for *in vivo* experiments. MK-801 was purchased from Sigma Aldrich (St. Louis, MO) and dissolved in DMSO for the cell death assay and dissolved in saline for *in vivo* experiments. ZL006, used here in AlphaScreen as a positive control [27], was obtained from Dr. Ganesh Thakur (Northeastern University, MA) and dissolved in DMSO.

### 2.2 Protein purification

Purification of glutathione S-transferase (GST), His-tagged PSD95, nNOS and NOS1AP is previously described [27; 29]. In short, PSD95<sub>1-392</sub>, containing the PDZ domain that binds nNOS, was expressed as His-tagged using pET-30a. nNOS<sub>1-299</sub>, containing the core PDZ domain that binds NOS1AP and the  $\beta$ -finger that binds to PDZ2 of PSD95 but lacking the catalytic domain, was expressed as GST- or His-tagged using pGEX 4T-1 or pET-30a, respectively. GST-NOS1AP<sub>400-506</sub>, containing the internal ExF internal motif and C-terminal tail that is recognized by the core PDZ domain of nNOS, was expressed as GST-tagged.

### 2.3 AlphaScreen assay

AlphaScreen assays were set up and performed as previously described by our group [27]. AlphaScreen is a bead-based binding assay which uses donor beads, coated with glutathione, which recognize GST-tagged purified protein, and acceptor beads, coated with Nickel-chelate, which recognize His-tagged purified protein. When donor beads are excited with 680 nm light, phthalocyanine containing donor beads convert ambient oxygen into singlet oxygen. When two proteins are in close proximity (i.e. within 200 nm), thioxene derivatives containing acceptor beads receive singlet oxygen and emit light at 520–620 nm which can

then be read with an EnSpire<sup>®</sup> Multimode Plate Reader (PerkinElmer, Waltham, MA). Briefly, binding between nNOS and NOS1AP was set up using His-nNOS<sub>1-299</sub> and GST-NOS1AP<sub>400-506</sub> proteins. AlphaScreen Ni Chelate Acceptor beads (PerkinElmer, Waltham, MA) and AlphaScreen Glutathione Donor beads (PerkinElmer, Waltham, MA) were sequentially added, and incubated for 1 h with each addition. The reaction was carried out in a 40 µl final volume using 96-well ½ area plates in 1X PBS containing BSA (1mg/mL) and Tween-20 (0.1%). An EnSpire<sup>®</sup> Multimode Plate Reader (PerkinElmer, Waltham, MA) equipped with AlphaScreen optical detection module was used to read plates. Titration was performed to determine 50% binding (or K<sub>d</sub>) between His-nNOS<sub>1-299</sub> and GST-NOS1AP<sub>400-506</sub> (0–200 nM each). To test disruption of the protein-protein binding by short peptide inhibitors, the reaction was carried out using concentrations of His-nNOS<sub>1-299</sub> and GST-NOS1AP<sub>400-506</sub> that lead to 50% of maximum binding. Inhibitors or vehicle (i.e. serial dilutions were performed with PBS or DMSO in parallel with inhibitors) were added to the protein pairs at the beginning of the experiments. To confirm specificity of disruption, control experiments tested the ability of the short peptide inhibitors to disrupt binding between purified His-PSD95<sub>1-392</sub> and GST-nNOS<sub>1-299</sub> using the PSD95-nNOS inhibitor ZL006 as a positive control. All the short peptides used in this experiment were dissolved in 1X PBS. ZL006 was dissolved in DMSO (>99% purity, Sigma-Aldrich, St. Louis, MO). Peptides and ZL006 were prepared as 10 or 20 mM stocks and subsequent dilutions were made from this stock for use in each assay. In each assay, 1X PBS and DMSO, the vehicles used to dissolve the peptides and small molecules, respectively, were also subsequently diluted in the same manner as the test compounds. Peptides or ZL006 ranging in concentrations from 0–200 µM were used. The readout of each point from EnSpire<sup>®</sup> Multimode Plate Reader was normalized into %AlphaScreen Signal Counts with the following equation: (signal detected with drug treatment at X concentration/signal detected without drug treatment)\*100. Each data point represents the means derived from all replicates generated from at least two independent assays performed on separate days. IC<sub>50</sub> was determined by non-linear regression with equation of log (inhibitor) vs. normalized response.

#### 2.4 Embryonic cortical neuron culture

Timed-pregnant Sprague Dawley rats were obtained from Envigo (Indianapolis, IN) and, following equilibration in the animal facility, were sacrificed via decapitation after halothane administration to obtain embryonic pups for cell culture experiments. Cortices derived from E18-E19 Sprague-Dawley rat pups were harvested according to approved IACUC guidelines as previously described [3; 21]. Pelleted cortical cells were resuspended in neuronal growth (Neurobasal) media containing 2% NuSerum (BD Biosciences, San Jose, CA), 2% NS21, penicillin (10 units/mL), streptomycin (10 µg/mL), and L-glutamine (29.2 µg/mL) at a density of 2.5 million cells/mL and seeded on poly-D-lysine (50 µg/mL)- coated 15 mm coverslips (German glass Number 0). Forty-eight hours after plating, cultures were treated with 5-fluor-2'-deoxyuridine (1.5 µg/mL) and uridine (3.5 µg/mL) to minimize glial contamination [27].

## 2.5 Excitotoxic stimulation and cell death assay

Neurons (DIV 7–8) were pretreated with TAT-GESV (10  $\mu$ M), TAT-cp4GESV (10  $\mu$ M), the NMDAR antagonist MK-801 (20  $\mu$ M) or vehicle for 20 minutes at 37°C and subsequently treated with excitotoxic stimulants 100  $\mu$ M glutamate/10  $\mu$ M glycine for 1 h at 37 °C [3]. Following treatment, stimulation media was removed and coverslips were washed with fresh neuronal growth media and the neurons were incubated for 24 h. The coverslips were washed the next day in PBS and stained using Live/Dead Cytotoxicity/Viability kit (Molecular Probes, Eugene, OR). Following staining, the coverslips were washed in PBS and immediately imaged using a Nikon Ti-E inverted microscope (100X magnification). Each coverslip was imaged in three different fields using a Texas Red filter to detect cytotoxicity and a FITC filter to detect viable cells. Cells were quantified using the automated counting software Nikon Elements 3.0 [27].

## 2.6 Subjects

Adult C57BL/6J male mice, weighing 23–33g (Jackson Laboratory, Bar Harbor, ME) were used in these experiments. Adult mice were housed at Indiana University Bloomington in a temperature-controlled facility (73  $\pm$  2 °F, 45% humidity under a 12-hour light/dark cycle). The mice received standard rodent chow and water *ad libitum*. All experimental procedures were approved by Bloomington Institutional Animal Care and Use Committee of Indiana University and followed guidelines of the International Association for the Study of Pain. The experimenter was blinded to the experimental condition in all *in vivo* studies.

## 2.7 Paclitaxel-induced neuropathic pain

Paclitaxel (Tecoland Corporation, Irvine, CA) was dissolved in a vehicle consisting of a 1:1:4 ratio of cremophor EL (Sigma-Aldrich, St. Louis, MO): 95% ethanol (Sigma-Aldrich): saline (Aquilite System; Hospira, Inc, Lake Forest, IL). Mice were injected with either the cremophor-based vehicle (i.e. vehicle) or paclitaxel (4 mg/kg, i.p.) on day 0, 2, 4, and 6 following initiation of paclitaxel dosing (16 mg/kg i.p. cumulative dose). Responsiveness to mechanical and cold stimulation was assessed before initiation of paclitaxel or vehicle dosing (Baseline, day 0) and during development and maintenance phases of paclitaxel-induced hypersensitivity as previously described [27]. Sensitivity to mechanical and cold stimulation was assessed on days 4, 7, 11 and 15 following initial paclitaxel/vehicle dosing.

## 2.8 Dose response of nNOS-NOS1AP peptide inhibitors in paclitaxel-induced neuropathic pain model

Peptides or saline were administered using the method of direct intrathecal injection described by Fairbanks [16] and Wilcox [22]. Briefly, direct lumbar puncture was performed on conscious mice with a 30-gauge, 0.5 inch sterile disposable PrecisionGlide needle (BD, Franklin Lake, NJ) connected to a 50  $\mu$ l Luer-hub Hamilton syringe (Hamilton Robotics, Reno, NV). The needle was inserted at the midline between the hip bones which corresponds to the level of the cauda equina. Puncture of the dura was indicated by a “tail-flick” or formation of an “S” shape tail as described by Fairbanks [16]. No motor impairment was observed in any of the animals receiving intrathecal injections. The injection volume was 5  $\mu$ l. All intrathecal injections were performed by a single

experimenter with extensive prior training marked by greater than 90% success rate (i.e. resulting in “tail flick” or “S”-shaped tail) prior to initiation of experiments described in the present study. When paclitaxel-induced neuropathy was stable (i.e. beginning on day 16 post initiation of paclitaxel dosing), mice were randomly divided into six groups and injected with saline (i.t.), TAT-GESV (1.25, 2.5, 5 or 10 nmol i.t) or TAT-GESV p1 (10 nmol i.t). Mice receiving the cremophor-based vehicle were treated concurrently with the same peptide treatments to ascertain whether changes in mechanical or cold responsiveness required the presence of the neuropathic pain state. Responsiveness to mechanical and cold stimulation was assessed in the same animals beginning 10 minutes following i.t. injection of peptide or saline.

### **2.9 Time course of nNOS-NOS1AP peptide inhibitors in paclitaxel-induced neuropathic pain model**

A separate group of paclitaxel-treated mice were randomly divided into three groups and injected intrathecally with saline (i.t.), an efficacious dose of TAT-GESV (5 nmol i.t.) or TAT-GESV p1 (5 nmol i.t.) on day 16 following initiation of paclitaxel dosing. Responsiveness to mechanical and cold stimulation was assessed starting at 10 minutes after peptide injection and re-evaluated at 30, 60, 90, and 150 minutes post injection.

### **2.10 Assessment of mechanical allodynia**

Withdrawal thresholds (g) to mechanical stimulation were measured in duplicate for each paw using an electronic von Frey anesthesiometer supplied with a 90-g semi-flexible probe (IITC Life Science, Woodland Hills, CA) as described previously [14; 18]. Both paclitaxel- and PSNL-evoked allodynia were evaluated with this method.

### **2.11 Assessment of cold allodynia**

Responsiveness to cold was assessed by applying an acetone bubble (~5–6  $\mu$ l) (Sigma Aldrich, St. Louis, MO) to the plantar surface of the hind paw through the hub of a 1 cc syringe with no needle. Time spent reacting to acetone stimulation (i.e., raising shaking, licking or stepping) was measured in triplicate for each paw [14; 43; 51]. Both paclitaxel- and PSNL-evoked allodynia were evaluated with this method.

### **2.12 Partial sciatic nerve ligation model of traumatic nerve injury**

Prior to surgery, baseline responses to mechanical and cold stimulation were assessed. On the day of surgery, the right thigh of the animal was shaved and aseptic surgical procedures were followed. Under light anesthesia with isoflurane, the sciatic nerve was pierced with 8-0 silk black braided suture (Ethicon, Somerville, NJ) so that 1/3 to 1/2 of the right sciatic nerve of the animal could be isolated and tightly ligated with the suture as previously described to induce the partial sciatic nerve ligation (PSNL) model of neuropathic pain. Seven days post-surgery, responsiveness to mechanical and cold stimulation was reassessed. Animals were then divided into six groups receiving i.t. injections of saline, MK-801 (5 nmol i.t.), TAT-GESV (2.5, 5, and 10 nmol i.t.) or TAT-GESV p1 (10 nmol i.t.). Mechanical paw withdrawal thresholds and duration of time spent reacting to cold stimulation was evaluated 10 minutes following i.t. injection. The same mice subsequently received repeated once

daily intrathecal injections with the same saline, MK-801 (5 nmol i.t.), TAT-GESV (10 nmol i.t.) or TAT-GESV p1 (10 nmol i.t.) treatments delivered acutely for a total of 8 consecutive days. Mechanical and cold sensitivity were re-evaluated on days 4 and 8 following the initial intrathecal injection.

### 2.13 Rota-rod test

Motor performance was assessed as described previously using an accelerating Rota-rod (IITC Life Science) (4–40 rpm with cutoff time of 300 seconds). Mice were trained for two days and, on the third day, the baseline descent latency was measured. On the fourth day, mice were intrathecally injected with saline (i.t.), MK-801 (5, 10 or 25 nmol i.t.), TAT-GESV (10 nmol i.t.), or TAT-GESV 1 (10 nmol i.t.). Ten minutes after injection, the mice were placed on the accelerating rota-rod and the latency for the animals to fall off the rotating drum was recorded. On the baseline and post-drug testing day, each mouse was required to pass a criterion (i.e. ability to walk on the rotating drum for 30 seconds) in order to advance to assessment of drug effects. Mice (n = 4) that did not pass criteria did not receive any pharmacological manipulations and were not included in the study.

### 2.14 Radiant heat tail flick

The latency of tail withdrawal from radiant heat was assessed using an IITC Tail Flick Analgesia Meter (Model 336) (IITC Life Science Inc., Woodland Hills, CA). Cutoff time was set to 10 seconds to prevent damage to the tail of the mice. Baseline withdrawal latencies were measured in triplicate prior to pharmacological manipulations (i.e. approximately one day before the experimental day). The intensity of the radiant heat was set to obtain a baseline tail-flick latency of approximately 5 seconds. On the experimental day, mice were injected acutely with saline (i.t.), MK-801 (5–25 nmol i.t.), TAT-GESV (10 nmol i.t.) or TAT-GESV 1 (10 nmol i.t.) 10 minutes prior to tail flick assessment. Tail flick latencies were evaluated in duplicate following pharmacological manipulations using a six-minute interstimulation interval.

### 2.15 Generation of lumbar spinal cord samples for western blot analysis

A separate group of mice were injected with saline (i.t.), TAT-GESV (5 nmol i.t.) or TAT-GESV 1 (5 nmol i.t.) on day 16 following initial paclitaxel or vehicle treatment. Twenty minutes following intrathecal injection, at the time point where maximum anti-allodynic efficacy was observed in the paclitaxel model (as determined previously), mice were rapidly decapitated without anesthesia and the lumbar enlargement was rapidly dissected, fast frozen in isopentane precooled on dry ice and stored at –80°C until use. Lumbar spinal cord tissue was processed for pp38MAPK, pp53 and pERK1/2 analysis using western blot protocols described below.

### 2.16 Immunoblotting for pERK1/2, and pp53

Mouse lumbar spinal cords were homogenized in RIPA buffer (25mM Tris, 150mM NaCl, 0.1% SDS, 0.5% sodium deoxycholate, 1% Triton X-100, pH 7.4) supplemented with 1 mM DTT, 10 µg/ml protease inhibitors (aprotinin, leupeptin, and pepstatin A), 0.1 mg/ml PMSF, and precleared at 20,000 g for 10 minutes at 4 °C. Total protein was measured using a Bio-

Rad DC Protein Assay Kit (Bio-rad, Hercules, CA). The supernatant of each sample was boiled in SDS-PAGE sample loading buffer for 10 minutes at 95 °C and analyzed by Western blotting.

For Western blot analysis, samples were loaded onto SDS-PAGE gel and transferred to nitrocellulose membrane. Nitrocellulose membranes were blocked with TBS-T with 5% milk added. Antibodies used were as follows: Phospho-p53 (Ser 15) (D4S1H) rabbit mAb (#12571, Cell Signaling Technology, Danvers, MA.), Anti-ACTIVE® MAPK (pTEpY) rabbit polyclonal Ab (#V8031, Promega, Madison, WI.), p44/42 MAPK (Erk 1/2) rabbit polyclonal Ab (#9102, Cell Signaling Technology), THE™ beta Actin mouse mAb (#A00702, Piscataway, NJ), goat anti-rabbit-HRP (#sc-2030, Santa Cruz, Santa Cruz, CA) and goat anti-mouse-HRP (#sc-2005, Santa Cruz, Santa Cruz, CA). Blots were developed using SuperSignal West Femto Maximum Sensitivity substrate (ThermoFisher Scientific Waltham, MA) and pre-flashed (Sensitize unit, GE) X-ray films (Amersham Hyperfilm ECL, GE) were exposed to the blots. Images were quantified using Image J Gel Analyzer (Background corrected profile analysis).

## 2.17 Statistical Analysis

Data analyses were performed according to principles outlined by Motulsky [35]. All *in vitro* data was analyzed using GraphPad Prism version 7.0 (GraphPad Software, La Jolla, CA). Dose response curves derived from AlphaScreen data were analyzed by non-linear regression using the equation of an inhibitor (log) vs. normalized response to generate IC<sub>50</sub> values. Impact of drug treatments on glutamate/glycine-induced cell death was analyzed by One-way analysis of variance (ANOVA) followed by Bonferroni's *post hoc* tests. Results from immunoblotting experiments were analyzed by One-way ANOVA followed by either Bonferroni's multiple comparison tests (for pp53) or Bonferroni's *post hoc* tests (for pERK). Bonferroni's multiple comparison tests, which use the mean square result from the overall ANOVA table, were performed using GraphPad Prism 7.0. The multiple comparisons tests enable comparison of preselected pairs of means (i.e. TAT-GESV vs. saline and TAT-GESV vs. TAT-GESV 1) to obtain more statistical power to detect differences by making a more limited set of comparisons [35], thereby minimizing chances of obtaining a Type II error. *In vivo* data were analyzed using SPSS (SPSS Inc., an IBM company, Chicago, IL, USA). *In vivo* data involving more than two sets of data and only one variable (i.e. different drugs) were analyzed using one-way ANOVA followed by Bonferroni's *post hoc* tests. *In vivo* data involving two variables (e.g. compounds and time) were analyzed by either repeated measures two-way ANOVA (i.e. when behavioral measures were evaluated in the same animals at different times) or by two-way ANOVA (i.e. when behavioral measures were evaluated in different groups of animals), followed by Bonferroni's *post hoc* tests in each case. The impact of surgery (PSNL/sham) on mechanical and cold sensitivity relative to baseline (pre-surgery) was evaluated prior to intrathecal injections using two-way repeated measures ANOVA followed by Bonferroni's *post hoc* tests when these designs involved comparisons of more than two independent groups. Planned comparisons between two groups were performed using unpaired or paired sample t-tests, as appropriate for between group or within group comparisons, respectively.  $P < 0.05$  was considered statistically significant.



### 3. Results

#### 3.1 TAT-GESV specifically disrupts the nNOS-NOS1AP complex in an *in vitro* AlphaScreen binding assay

TAT-GESV disrupted protein-protein interactions between His-nNOS<sub>1-299</sub> and GST-NOS1AP<sub>400-506</sub> in an AlphaScreen biochemical binding assay with an IC<sub>50</sub> of 8.47 μM (Figure 1A). TAT and PBS did not interfere with the binding between His-nNOS<sub>1-299</sub> and GST-NOS1AP<sub>400-506</sub> (Figure 1A). In addition to TAT-GESV 1, we also included TAT-cp4GESV, which did not disrupt NMDA activation-induced cell death in our previous work [29], as a negative control. Neither TAT-cp4GESV nor TAT-GESV 1 disrupted the interactions between His-nNOS<sub>1-299</sub> and GST-NOS1AP<sub>400-506</sub> in AlphaScreen (Figure 1A). Moreover, TAT-GESV did not disrupt the binding between purified GST-nNOS<sub>1-299</sub> and His-PSD95<sub>1-392</sub> (Figure 1B), suggesting that the active peptide did not disrupt the interactions between PDZ2 of PSD95 and the β-finger flanking the nNOS core PDZ domain. However, the PSD95-nNOS small molecule inhibitor ZL006 reliably disrupted the binding between purified GST-nNOS<sub>1-299</sub> and His-PSD95<sub>1-392</sub> with IC<sub>50</sub> of 12.76 μM (Figure 1B), similar to what was described previously by our group [27].

#### 3.2 TAT-GESV protects against glutamate/glycine-induced cell-death

To verify that disruption of nNOS-NOS1AP interaction inhibits NMDAR-dependent excitotoxicity, we characterized the efficacy of TAT-GESV in protecting against glutamate-induced neuronal cell death. In primary cortical neurons, addition of glutamate (100 μM)/glycine (10 μM) for 1 h produced cell death that differed between the experimental treatments [ $F_{4,13} = 75.376$ ;  $p < 0.0001$ , one-way ANOVA] (Figure 2). Cell death was higher in primary cortical neurons pre-treated with vehicle that were exposed to glutamate/glycine compared to the control (no glutamate/glycine) condition [ $p < 0.001$ , Bonferroni's *post hoc* test]. Pretreatment of cortical neurons with either the nNOS-NOS1AP disruptor TAT-GESV (10 μM) or the NMDAR antagonist MK-801 (20 μM) attenuated glutamate/glycine-induced cell death relative to vehicle [ $p < 0.001$  for each comparison, Bonferroni's *post hoc* test]. Cell death was lower in primary cortical neurons pre-treated with the active peptide TAT-GESV compared to the inactive peptide TAT-cp4GESV [ $p < 0.001$ , Bonferroni's *post hoc* test]). TAT-cp4GESV did not protect against glutamate/glycine-induced cell-death relative to vehicle [ $p = 1$ , Bonferroni's *post hoc* test]. Cell death was lower in primary cortical neurons pre-treated with MK-801 compared to all other groups exposed to glutamate/glycine [ $p < 0.01$  for each comparison, Bonferroni's *post hoc* test]. Glutamate/glycine-induced cell death was higher in primary cortical neurons pre-treated with either vehicle or TAT-cp4GESV compared to all other groups [ $p < 0.001$  for each comparison, Bonferroni's *post hoc* test] (Figure 2).

#### 3.3 Intrathecal TAT-GESV dose-dependently reduces paclitaxel-induced neuropathic pain

We treated mice with paclitaxel or its vehicle and evaluated whether intrathecal administration of TAT-GESV would suppress paclitaxel-induced neuropathic pain (see Figure 3A). Prior to treatment with paclitaxel or vehicle, there were no differences between groups in paw withdrawal thresholds to mechanical stimulation [ $p = 0.68$ , unpaired t-test; Figure 3B] or duration of responsiveness to cold stimulation [ $p = 0.421$ , unpaired t-test;

Figure 3C]. Paclitaxel decreased mechanical paw withdrawal thresholds, mechanical responsiveness differed across test days and the effects of paclitaxel were time-dependent [ $F_{1,70} = 265.136$ ;  $p < 0.0001$  (treatment);  $F_{4,280} = 84.744$ ;  $p < 0.0001$  (time);  $F_{4,280} = 90.28$ ;  $p < 0.0001$  (interaction); two-way repeated measures ANOVA; Figure 3B]. Paclitaxel also increased the duration of responding to cold, cold responsiveness differed across test days and the effects of paclitaxel on cold responsiveness were also time dependent [ $F_{1,70} = 117.271$ ;  $p < 0.0001$  (treatment);  $F_{4,280} = 79.966$ ;  $p < 0.0001$  (time);  $F_{4,280} = 69.587$ ;  $p < 0.0001$  (interaction); two-way repeated measures ANOVA; Figure 3C]. Paclitaxel lowered mechanical paw withdrawal thresholds and increased cold response times relative to vehicle starting on day 7 and these behavioral hypersensitivities remained ongoing on day 15 post injection [mechanical and cold:  $p < 0.0001$  from day 7–15, Bonferroni's *post hoc* test] (Figure 3B,C).

On day 16, mice received direct intrathecal injections of saline, TAT-GESV, or TAT-GESV 1 (Figure 3A). Prior to intrathecal injections (day 16), paclitaxel reduced mechanical thresholds relative to baseline (pre-injection) levels [ $p < 0.0001$ , paired sample t-test; Figure 3D] whereas the cremophor-based vehicle had no such effect [ $p = 0.975$ , paired sample t-test; Figure 3D]. Similarly, mechanical paw withdrawal thresholds were lower in paclitaxel-treated compared to vehicle-treated mice on day 16, prior to intrathecal injections [ $p < 0.0001$ , unpaired t-test; Figure 3D]. Intrathecal TAT-GESV treatment elevated mechanical paw withdrawal thresholds, the doses differed from each other and the interaction between dose and treatment was significant [ $F_{1,50} = 123.426$ ,  $p < 0.0001$  (treatment);  $F_{4,50} = 13.267$ ,  $p < 0.0001$  (dose);  $F_{4,50} = 12.474$ ,  $p < 0.0001$  (interaction): Two-way ANOVA]. TAT-GESV (5 nmol, i.t.) restored paw withdrawal thresholds in paclitaxel-treated mice to the level observed in vehicle-treated mice receiving the same dose [ $p = 0.654$ , Bonferroni's *post hoc* test] (Figure 3D). Lower doses of TAT-GESV (1.25 and 2.5 nmol) did not normalize paw withdrawal thresholds to levels observed in vehicle-treated mice receiving the same doses [ $p = 0.0001$ , Bonferroni's *post hoc* test] (Figure 3D).

In paclitaxel-treated mice, TAT-GESV (10 nmol, i.t) increased paw withdrawal thresholds [ $F_{2,15} = 13.823$ ,  $p < 0.001$ ; One-way ANOVA] compared to either saline (i.t.) [ $p = 0.001$ , Bonferroni's *post hoc* test] or TAT-GESV 1 [ $p = 0.003$ , Bonferroni's *post hoc* test] treatments. Effects of TAT-GESV 1 (10 nmol, i.t.) [ $p = 1$ , Bonferroni's *post hoc* test] did not differ from saline (i.t.) treatment (Figure 3F).

Prior to intrathecal injections (day 16), paclitaxel increased duration of responding to cold stimulation relative to baseline levels [ $p < 0.0001$ , paired sample t-test] whereas the cremophor-vehicle had no such effect [ $p = 0.264$ , paired sample t-test] (Figure 3E). Intrathecal administration of TAT-GESV reduced cold responses, the doses differed from each other and the interaction between dose and treatment was significant [ $F_{1,50} = 72.183$ ,  $p < 0.0001$  (treatment);  $F_{4,50} = 7.15$ ,  $p < 0.0002$  (dose);  $F_{4,50} = 6.09$ ,  $p < 0.0005$  (interaction): Two-way ANOVA]. Paclitaxel-induced cold responsiveness was dose-dependently reduced by TAT-GESV and the 5 nmol (i.t.) dose normalized cold response times to levels observed in vehicle-treated mice receiving the same dose [ $p = 0.215$ , Bonferroni's *post hoc* test] (Figure 3E). Other doses of TAT-GESV (1.25, 2.5 and 10 nmol) failed to normalize cold response times compared to vehicle-treated mice receiving the same doses [ $p < 0.05$  for each

comparison, Bonferroni's *post hoc* test] (Figure 3E). Effects of the 5 nmol and 10 nmol doses of TAT-GESV on either mechanical or cold responsiveness did not differ from each other [ $p = 1$ , Bonferroni's *post hoc* test] (Figure 3D, E).

In paclitaxel-treated mice, TAT-GESV (10 nmol i.t.) reduced cold response times [ $F_{2,15} = 4.241$ ,  $p < 0.05$ ; One-way ANOVA] relative to saline [ $p = 0.039$ , Bonferroni's *post hoc* test] but not TAT-GESV 1 (10 nmol, i.t.) [ $p = 0.172$ , Bonferroni's *post hoc* test] (Figure 3G). However, effects of TAT-GESV 1 did not differ from saline [ $p = 1$ , Bonferroni's *post hoc* test].

### 3.4 Time course of TAT-GESV-induced suppression of paclitaxel-induced mechanical allodynia

The duration of anti-allodynic efficacy of TAT-GESV was evaluated in a separate set of paclitaxel-treated mice. Intrathecal drug treatments altered paclitaxel-induced mechanical hypersensitivity (Figure 4). No main effect of time was observed and the interaction between intrathecal treatment and time was significant [ $F_{2,12} = 22.252$ ,  $p < 0.001$  (group);  $F_{5,60} = 1.426$ ,  $p = 0.228$  (time);  $F_{10,60} = 3.584$ ,  $p < 0.002$  (interaction); Two-way repeated measures ANOVA] (Figure 4). The maximally efficacious dose of TAT-GESV (5 nmol, i.t.) increased paw withdrawal thresholds compared to either saline [ $p < 0.0001$ , Bonferroni's *post hoc* test] or TAT-GESV 1 [ $p = 0.003$ , Bonferroni's *post hoc* test] throughout the observation interval, whereas effects of TAT-GESV 1 did not differ from saline [ $p = 0.154$ , Bonferroni's *post hoc* test]. TAT-GESV reliably increased mechanical paw withdrawal thresholds in paclitaxel-treated mice relative to the saline-treated group from 10 to 60 min post-injection [10–60 min:  $p < 0.009$  for all comparisons, Bonferroni's *post hoc* test] (Figure 4). Paw withdrawal thresholds were higher in mice receiving the active compared to the inactive peptide from 10–30 min post injection [10 min:  $p < 0.04$ ; 30 min:  $p < 0.0002$ ; Bonferroni's *post hoc* test] (Figure 4). By contrast, TAT-GESV 1 (5 nmol, i.t.) did not alter paclitaxel-induced mechanical responsiveness relative to saline (i.t.) [ $p > 0.363$  for all time points, Bonferroni's *post hoc* test] (Figure 4).

### 3.5 Intrathecal TAT-GESV reduces paclitaxel-induced p53 activation but not ERK1/2 activation in mouse lumbar spinal cord

Phosphorylated p38 MAPK (p-p38 MAPK, used as a measure of activated p38 MAPK) was not reliably detected in mouse lumbar spinal cord tissue at the time point when the tissue was collected (unpublished observations). We asked, therefore, whether lumbar spinal cord levels of phosphorylation of p53 at serine 15 (pSer15-p53), a residue at p53 selectively phosphorylated by activated p38 MAPK, could be more abundant and, therefore, detectable under conditions in which the active kinase was not. Using the same tissue used for p-p38MAPK detection, we compared pSer15-p53 levels in lumbar spinal cords derived from paclitaxel-treated mice receiving TAT-GESV (5 nmol i.t.), TAT-GESV 1 (5 nmol i.t.) or saline (i.t.) with vehicle-treated mice receiving saline (i.t.); the overall ANOVA approached significance [ $F_{3,16} = 2.851$ ,  $p = 0.07$ ; One-way ANOVA; Figure 5A,C]. Bonferroni's multiple comparison test, which uses the mean square error term from this same ANOVA table [35], nonetheless, revealed that TAT-GESV reduced pSer15-p53 levels compared to saline [ $p < 0.05$ ] but not compared to TAT-GESV 1 [ $p = 0.16$ ] treatment. We also asked

whether pSer15-p53 levels were increased by paclitaxel treatment in a manner blocked by spinal disruption of nNOS-NOS1AP interactions. Paclitaxel increased lumbar spinal cord levels of pSer15-p53 in a TAT-GESV-sensitive manner [ $F_{2,12} = 17.447$ ,  $p < 0.0003$ , One-way ANOVA]; pSer15-p53 levels were increased in samples derived from paclitaxel-treated compared to vehicle-treated mice [ $p = 0.002$ , Bonferroni's *post hoc* test] and TAT-GESV (5 nmol i.t.) also reduced paclitaxel-induced elevations in pSer15-p53 levels [ $p = 0.0004$ , Bonferroni's *post hoc* test]. Lumbar spinal cord pSer15-p53 levels did not differ in samples derived from cremophor vehicle-treated mice that received saline (i.t.) and paclitaxel-treated mice receiving TAT-GESV (i.t.) [ $p = 1$ , Bonferroni's *post hoc* test], suggesting that TAT-GESV effectively restored pSer15-p53 levels to normal (Figure 5A,C). We also evaluated phosphorylation levels of another MAPK group, ERK1/2, because these kinases can also phosphorylate p53 at Ser15 [37; 41]. Paclitaxel elevated pERK1/2 levels [ $F_{3,16} = 60.34$ ;  $p < 0.0001$ , One-way ANOVA] in the same lumbar spinal cord samples evaluated for pSer-p53 levels relative to those derived from cremophor-vehicle treated mice similarly receiving saline (i.t.) [ $p < 0.0001$ , Bonferroni's *post hoc* test]. However, in samples derived from paclitaxel-treated mice, neither TAT-GESV nor TAT-GESV 1 (5 nmol, i.t.) altered pERK1/2 elevation relative to saline (i.t.) [ $p > 0.4$ , Bonferroni's *post hoc* test] (Figure 5B,D). These observations suggest that the TAT-GESV-induced blockade of pSer15-p53 phosphorylation induced by paclitaxel in lumbar spinal cord is independent of the ERK1/2 pathway (Fig. 5A–D).

### 3.6 Intrathecal TAT-GESV attenuates neuropathic pain induced by partial sciatic nerve ligation

To determine whether TAT-GESV suppresses neuropathic pain induced by a surgically-induced traumatic nerve injury, we subjected mice to unilateral PSNL or sham surgery (see Figure 6A). Unilateral PSNL reduced mechanical paw withdrawal thresholds and increased duration of responding to cold in the injured (ipsilateral) paw relative to baseline (pre-surgery) levels [mechanical:  $p < 0.0001$ ; cold:  $p < 0.0001$ , paired sample t-test] (Figure 6B,C). By contrast, sham surgery did not alter responsiveness to mechanical or cold stimulation relative to baseline (pre-surgery) levels [Mechanical:  $p = 0.159$ ; Cold:  $p = 0.416$ , paired sample t-test] (Figure 6B,C).

Post-injection paw withdrawal thresholds differed between PSNL and sham-operated groups, the TAT-GESV doses differed from each other and the interaction between dose and surgical treatment was significant [ $F_{1,56} = 24.532$ ,  $p < 0.0001$  (group);  $F_{3,56} = 3.694$ ,  $p = 0.017$  (dose);  $F_{3,56} = 3.673$ ,  $p = 0.017$  (interaction); Two-way ANOVA] (Figure 6B). TAT-GESV (5 and 10 nmol i.t.) elevated mechanical paw withdrawal thresholds in the ipsilateral paw of PSNL-operated mice, normalizing responsiveness to levels observed in sham-operated mice receiving the same doses [5 nmol:  $p = 0.261$ ; 10 nmol:  $p = 0.474$ , Bonferroni's *post hoc* test] (Figure 6B). By contrast, ipsilateral paw withdrawal thresholds were lower in PSNL-treated mice receiving vehicle [0 nmol;  $p < 0.0001$ , Bonferroni's *post hoc* test] or the low dose of TAT-GESV (2.5 nmol i.t.) [ $p = 0.001$ , Bonferroni's *post hoc* test] compared to sham-operated mice receiving the same treatments (Figure 6B).

Post-injection cold response times also trended to differ between PSNL- and sham-operated groups, the TAT-GESV doses differed from each other and the interaction between dose and surgical treatment was significant [ $F_{1,56} = 3.067$ ,  $p = 0.085$  (group);  $F_{3,56} = 6.28$ ,  $p = 0.001$  (dose);  $F_{3,56} = 5.426$ ,  $p = 0.002$  (interaction); Two-way ANOVA] (Figure 6C). TAT-GESV, at doses of 2.5, 5 and 10 nmol (i.t.) [ $p > 0.072$  for each comparison, Bonferroni's *post hoc* test], normalized cold responsiveness to levels comparable to those observed in the sham-operated mice receiving the same doses (Figure 6C). By contrast, cold responsiveness in the ipsilateral paw was higher in PSNL-treated compared to sham-operated mice receiving saline (i.t.) [0 nmol;  $p < 0.0001$ , Bonferroni's *post hoc* test; Figure 6C].

In PSNL-treated groups, TAT-GESV (10 nmol, i.t.) increased paw withdrawal thresholds [ $F_{2,19} = 5.938$ ,  $p = 0.01$ ; One-way ANOVA] compared to either saline (i.t.) treatment or TAT-GESV 1 (10 nmol i.t.) treatment [ $p < 0.05$  for each comparison, Bonferroni's *post hoc* test] (Figure 6D). By contrast, paw withdrawal thresholds did not differ between PSNL-treated groups receiving TAT-GESV 1 (10 nmol, i.t.) or saline (i.t.) [ $p = 1$ , Bonferroni's *post hoc* test] (Fig. 6D).

In PSNL-operated mice, TAT-GESV (10 nmol i.t.) similarly reduced cold-response times [ $F_{2,19} = 10.633$ ,  $p = 0.001$ ; One-way ANOVA] compared to either saline (i.t.) [ $p < 0.01$ , Bonferroni's *post hoc* test] or TAT-GESV 1 (10 nmol) [ $p = 0.003$ , Bonferroni's *post hoc* test] treatment (Figure 6E). By contrast, cold responsiveness did not differ between PSNL-treated groups receiving TAT-GESV 1 (10 nmol, i.t.) and saline (i.t.) [ $p = 1$ , Bonferroni's *post hoc* test] (Figure 6E).

Surgical manipulations did not alter behavioral responding in the contralateral (non-operated) paw and no significant main effects or interactions were observed in the paw contralateral to PSNL or sham surgery for either stimulus modality [Mechanical:  $p = 0.168$  (group);  $p = 0.179$  (interaction); Cold:  $p = 0.941$  (group);  $p = 0.289$  (interaction); Two-way repeated measures ANOVA] (Figure 6F,G). Moreover, neither TAT-GESV nor TAT-GESV 1 altered mechanical or cold responsiveness in the paw contralateral to PSNL or sham surgery [Mechanical:  $p = 0.065$  (dose);  $p = 0.882$  (drug);  $p = 0.065$  (interaction); Cold:  $p = 0.39$  (dose);  $p = 0.491$  (drug);  $p = 0.882$  (interaction); Two-way ANOVA] (Figure 6F,G).

### 3.7 Impact of chronic intrathecal dosing with TAT-GESV on PSNL-induced mechanical and cold allodynia

Prior to intrathecal injections, PSNL surgery decreased mechanical paw withdrawal thresholds and increased cold response times relative to baseline [mechanical:  $F_{1,24} = 209.884$ ,  $p < 0.0001$ ; cold:  $F_{1,24} = 44.14$ ,  $p < 0.0001$ ; Two-way repeated measures ANOVA; Figure 7A,B]. There were no differences between groups prior to intrathecal treatments and the interaction between drug treatment and surgical condition was not significant [mechanical:  $p = 0.303$  (group),  $p = 0.625$  (interaction); cold:  $p = 0.811$  (group)  $p = 0.619$  (interaction); Two-way repeated measures ANOVA].

Post-injection mechanical paw withdrawal thresholds also differed between groups and across injection days and effects of intrathecal treatments were injection day dependent [ $F_{3,19} = 21.892$ ,  $p < 0.0001$  (group);  $F_{3,57} = 16.401$ ,  $p < 0.0001$  (day);  $F_{9,57} = 3.581$ ,  $p =$

0.001 (interaction); Two-way repeated measures ANOVA] (Figure 7A). Both TAT-GESV and MK-801 increased mechanical paw withdrawal thresholds relative to either saline (i.t.) or TAT-GESV 1 (i.t.) treatment throughout the chronic dosing period [ $p < 0.002$  for each comparison, Bonferroni's *post hoc* test] (Figure 7A). Effects of TAT-GESV did not differ from MK-801 (i.t.) and effects of TAT-GESV 1 (i.t.) did not differ from saline (i.t.) [ $p = 1$  for each comparison; Bonferroni's *post hoc* test] (Figure 7A). In mice subjected to PSNL, both TAT-GESV (i.t.) and MK-801 (i.t.) similarly increased mechanical paw withdrawal thresholds relative to saline (i.t.) or TAT-GESV 1 (i.t.) with sustained efficacy [day 4–8:  $p < 0.001$  for each comparison; Bonferroni's *post hoc* test] (Figure 7A).

In mice subjected to PSNL, cold response times differed between treatment groups and across injection days but this latter effect was not dependent upon drug treatment [ $F_{3,19} = 4.696$ ,  $p = 0.013$  (group);  $F_{3,57} = 3.359$ ;  $p = 0.025$  (day);  $F_{9,57} = 1.684$ ,  $p = 0.114$  (interaction), respectively; Two-way repeated measures ANOVA] (Figure 7B). In PSNL groups, TAT-GESV (i.t.) reduced cold responsiveness relative to saline (i.t.) treatment throughout the observation interval [ $p < 0.05$ ; Bonferroni's *post hoc* test], whereas reductions in cold sensitivity produced by MK801 approached significance [ $p = 0.072$ ; Bonferroni's *post hoc* test]. TAT-GESV 1 (i.t.) did not reliably alter cold responsiveness relative to saline (i.t.), MK-801 (i.t.) or TAT-GESV (i.t.) across the observation interval [ $p > 0.25$  for each comparison; Bonferroni's *post hoc* test] (Figure 7B).

In mice subjected to PSNL, repeated intrathecal dosing did not alter mechanical paw withdrawal thresholds or cold response times in the contralateral (unoperated) paw [mechanical:  $p = 0.332$  (group);  $p = 0.621$  (day);  $p = 0.92$  (interaction); Cold:  $p = 0.123$  (group);  $p = 0.171$  (day);  $p = 0.559$  (interaction); Two-way repeated measures ANOVA] (Figure 7C,D). In sham-operated mice, injection day impacted mechanical and cold responsiveness on the operated side [mechanical:  $F_{3,57} = 6.292$ ,  $p = 0.001$  (day); Cold:  $F_{3,57} = 3.376$ ,  $p = 0.024$  (day); Two-way repeated measures ANOVA], but these effects were not related to intrathecal treatments because no main effect of drug treatment was observed and the interaction between drug treatment and injection day was not significant [mechanical:  $p = 0.2$  (group);  $p = 0.124$  (interaction); cold:  $p = 0.649$  (group);  $p = 0.927$  (interaction); Two-way repeated measures ANOVA] (Figure 7E,F). Similarly, in mice subjected to sham surgeries, mechanical and cold responsiveness in the contralateral paw did not differ between groups or across injection days [mechanical:  $p = 0.12$  (group);  $p = 0.254$  (day);  $p = 0.837$  (interaction); cold:  $p = 0.831$  (group);  $p = 0.106$  (day);  $p = 0.77$  (interaction); Two-way repeated measures ANOVA] (Figure 7G,H).

### 3.8 Intrathecal TAT-GESV does not produce motor ataxia

Rota-rod descent latencies differed between groups in an injection-dependent manner [ $F_{5,28} = 2.785$ ;  $p = 0.037$  (interaction); Two-way repeated measures ANOVA] (Figure 8). The high dose of MK-801 (25 nmol i.t.) lowered rota-rod descent latencies relative to all other post-injection groups [ $p < 0.05$  for all comparisons; Bonferroni's *post hoc* test]. There were no main effects of either injection phase or drug treatment [ $F_{1,28} = 0.001$ ,  $p = 0.981$  (injection phase);  $F_{5,28} = 2.216$ ,  $p = 0.081$  (group); Two-way repeated measures ANOVA] (Figure 8).

### 3.9 Intrathecal TAT-GESV administration did not alter radiant heat tail flick latency

Tail-flick latencies did not differ between groups (Figure 9). Injections produced a modest but reliable increase in tail-flick latencies but this effect was independent of drug treatment because the interaction between injection phase and treatment group was not significant [ $F_{5,28} = 0.746$ ,  $p = 0.595$  (group);  $F_{1,28} = 5.405$ ,  $p = 0.028$  (injection phase);  $F_{5,28} = 0.615$ ,  $p = 0.689$  (interaction); Two-way repeated measures ANOVA]. Neither pre-injection tail-flick latencies [ $p = 0.879$ , One-way ANOVA] nor post-injection tail-flick latencies [ $p = 0.504$ , One-way ANOVA] differed between groups (Figure 9).

### 3.10 Summary of the effects of nNOS-NOS1AP disruption on pathological pain

A conceptual model summarizing the proposed effect of the membrane-permeant nNOS-NOS1AP disruptor TAT-GESV on NMDAR signaling in neuropathic pain is shown in Figure 10.

## Discussion

Here, we show that disrupting nNOS-NOS1AP interactions at the spinal level suppresses mechanistically distinct forms of neuropathic pain. Moreover, the nNOS-NOS1AP protein-protein interface may be implicated in pronociceptive signaling. We and others have shown that the NMDAR-PSD95-nNOS complex is a possible target for drug development of anti-hyperalgesic and anti-allodynic agents that lack unwanted side effects associated with NMDAR antagonists [8; 13; 17; 27; 44]. Disrupting protein-protein interactions downstream of NR2B produces therapeutic efficacy [8; 17; 27; 34; 56]. Tat-NR2B9c, a peptide comprising the last 9 a.a. of NR2B, shows therapeutic efficacy for stroke and neuropathic pain [1; 13; 20]. Moreover, among other Tat-NR2B9c interacting proteins, neuroprotective effects only resulted from suppressing the expression of PSD95 or nNOS, suggesting that NMDAR-PSD95-nNOS is critical in mediating NMDAR-dependent excitotoxicity [12].

Our group previously showed that NMDAR activation increases association of nNOS with its adaptor protein, NOS1AP, and this increased association leads to cell death through a p38 MAPK-dependent mechanism that is blocked by TAT-GESV, L-TAT-NR2B9c and IC87201 [29]. These findings suggest that p38 MAPK activation is linked to NMDAR activation and is blocked by disrupting NR2B-PSD95-nNOS-NOS1AP complexes. nNOS-NOS1AP disruption blocked NMDAR-mediated p38 MAPK activation without altering NO production, whereas disruption of NR2B-PSD95 and PSD95-nNOS reduced NO production [1; 7; 17; 23; 29; 39]. Thus, blockade of p38 MAPK activation may underly the neuroprotective efficacy of TAT-GESV. Therefore, we hypothesized that blocking the activation of NMDAR-mediated p38 MAPK activation through nNOS-NOS1AP disruption would represent a more functionally selective attenuation of neurotoxicity and pronociceptive signaling compared to targeting the upstream PSD95-nNOS or NR2B-PSD95 protein-protein interactions. We, therefore, evaluated whether disrupting nNOS-NOS1AP interactions could attenuate neuropathic pain and represent a potential therapeutic target for drug development of anti-allodynic agents.

We demonstrated the ability of the peptide inhibitor TAT-GESV to disrupt nNOS-NOS1AP interactions through a direct mechanism using AlphaScreen. TAT-GESV, but not the putative inactive peptides TAT-cp4GESV and TAT-GESV<sup>1</sup>, disrupted the binding between purified nNOS and NOS1AP. Our results are consistent with the previous finding derived from co-immunoprecipitation because TAT-GESV competes with NOS1AP for the C-terminal ligand binding site on nNOS PDZ, destabilizing nNOS-NOS1AP interactions [29; 30]. Moreover, deletion of the C-terminal valine in TAT-GESV<sup>1</sup>, by eliminating the strong hydrogen-bond and hydrophobic interactions with the nNOS PDZ domain, could account for our observation that TAT-GESV<sup>1</sup> failed to disrupt nNOS-NOS1AP binding.

We also verified the specificity of TAT-GESV in disrupting the nNOS-NOS1AP complex using AlphaScreen. TAT-GESV disrupted the binding between nNOS and NOS1AP but not between PSD95 and nNOS whereas the PSD95-nNOS inhibitor ZL006 reliably blocked the latter interaction [27]. nNOS interacts with PSD95 through its  $\beta$ -finger, while nNOS binds to NOS1AP at a site distinct from that of PSD95 [47; 48; 50]. Moreover, TAT-GESV is a consensus ligand (G-D/E-X-V) for the class III PDZ domain and does not correspond to the class I motif, conforming to D/E-T/S-X-V, with selectivity for PDZ domains like PDZ2 of PSD95 [29; 40; 47; 48]. These observations support the hypothesis that TAT-GESV disrupts nNOS-NOS1AP but not PSD95-nNOS interactions.

TAT-GESV has been shown to attenuate NMDA-induced cell death and block NMDA-induced activation of p38 MAPK [29]. We previously showed that small molecule PSD95-nNOS disruptors protect against glutamate-induced cell death in primary cortical neurons [27]. In the current study, TAT-GESV- or MK-801-pretreated cortical neurons were protected from glutamate/glycine-induced cell death whereas a putative inactive peptide had no effect. Collectively, our results confirm that TAT-GESV penetrates cells to disrupt NMDAR activation-mediated excitotoxicity [29].

The present studies demonstrate that disrupting nNOS-NOS1AP interactions with TAT-GESV suppresses behavioral hypersensitivities in two mechanistically distinct models of neuropathic pain: a model of toxic neuropathy induced by the chemotherapeutic agent paclitaxel and a model of traumatic nerve injury induced by PSNL. Chemotherapeutic agents can produce distal axonal injury and partial degeneration of the intraepidermal nerve fibers by affecting the excitability and survival of neurons through multiple mechanisms including disruption of axonal transport, increased ion channel activity, neuronal injury and inflammation [4; 19; 42; 54]. By contrast, PSNL results from direct injury and possible contributions from sympathetic sprouting and is regarded as having less of an inflammatory component than other peripheral nerve injury models [5]. In our studies, intrathecal administration of TAT-GESV, but not the inactive peptide TAT-GESV<sup>1</sup>, reversed mechanical and cold hypersensitivities in both neuropathic pain models. These observations support our hypothesis that disrupting nNOS-NOS1AP interactions is a viable anti-allodynic strategy for suppressing neuropathic pain.

We previously reported that PSD95-nNOS inhibitors IC87201 and ZL006, administered acutely, are efficacious in suppressing paclitaxel-induced neuropathic pain [27]. Here we show that paclitaxel-induced mechanical and cold allodynia is attenuated by both acute and



chronic TAT-GESV (i.t.), whereas basal nociceptive responses were not affected. Thus, nNOS-NOS1AP disruption eliminated aberrant mechanical and cold hypersensitivities induced by paclitaxel without altering normal nociception. Disrupting nNOS-NOS1AP interactions with nNOS<sub>1-99</sub> does not alter the enzymatic activity of nNOS or the production of NO whereas TAT-GESV blocked phosphorylation of p38 MAPK in cultured cells [6; 29]. We, therefore, collected lumbar spinal cords derived from paclitaxel-treated mice to determine whether TAT-GESV (i.t.) could attenuate p38 MAPK activation associated with a pathological pain state. Entire lumbar enlargements derived from paclitaxel-treated mice were used for parallelism with the *in vivo* studies and to enable us to eliminate variability in dissections. This sampling method would, nonetheless, be expected to dilute our signal because both dorsal and ventral horns were processed together in a single sample. We were unable to reliably detect p38 MAPK activity in these samples. Consistent with our finding, lumbar spinal cords derived from paclitaxel-treated rats did not exhibit increases in various microglia markers or phosphorylated p38 MAPK expression but exhibited increases in the astrocyte marker GFAP in spinal dorsal horn [53]. However, other studies have shown that NMDA administration directly to the spinal cord induced p38 MAPK activation, likely in microglia and a small subpopulation of neurons in rats [45]. In addition, administration of substance P and formalin in rats induced p38 MAPK activation in microglia 5 minutes post treatment but the activation returned to basal levels after 20 minutes [46]. Thus, the possibility remains that p38 MAPK is activated transiently in lumbar spinal cord after inflammatory insults or toxic challenge with paclitaxel. We, nonetheless, were able to demonstrate that phosphorylation of a selective substrate site for p38 MAPK, p53 at Ser15, a transcriptional regulator linked to cellular stress and chronic inflammation, was reliably increased in paclitaxel-treated lumbar spinal cords in a TAT-GESV-dependent manner. We found increases in pSer15-p53 level after paclitaxel compared to vehicle-treatment; this increase in pSer15-p53 expression was reduced in mice injected with TAT-GESV (i.t.). Moreover, ERK1/2, another upstream regulator of p53 reported to phosphorylate the same site (Ser 15) in ovarian carcinoma cells and in JB6 mouse epidermal cell line C1 41, was also activated by paclitaxel treatment, but TAT-GESV did not reduce this activation. Our findings suggest that the TAT-GESV-induced reduction of pSer15-p53 may partly result from disruption of p38 MAPK activation but not from reduced activity of ERK1/2. However, more work is needed to investigate the role of p53 in contributing to pathogenesis of paclitaxel-induced neuropathic pain.

TAT-GESV also produced anti-allodynic efficacy in a model of traumatic nerve injury. Intrathecal TAT-GESV dose-dependently reduced mechanical and cold allodynia in the paw ipsilateral to PSNL but did not alter basal nociceptive responses in controls. Effects were similar to those produced by MK-801. PSNL also activates astrocytes and microglia in the lumbar spinal dorsal horn of rats [10; 32] and mice [52]. However, disagreement exists as to whether p38 MAPK activation in the lumbar spinal cord is produced by PSNL, although species differences and signal detection time may contribute to experimental differences observed [32; 33; 52]. PSNL also increased mRNA expression of chemokines C-C motif ligand 1 (CCL-1) in mouse spinal cord and dorsal root ganglion (DRG) and direct intrathecal injections of CCL-1 also induced phosphorylation of NR1 and NR2B and activated astrocytes and microglia in the lumbar spinal cord [2]. Thus, CCL-1 may be the

key mediator of tactile allodynia induced by PSNL, presumably via modulation of both glial cell activation and glutamate transmission [2]. More work is necessary to determine which cell types underlie the anti-allodynic efficacy of TAT-GESV in the PSNL model and whether TAT-GESV also acts indirectly to reduce glial cell activation. Notably, high dose TAT-GESV (10 nmol, i.t.) did not produce motor impairment or alter normal nociception (i.e. produce tail flick antinociception or sensitization). By contrast, MK-801 (25 nmol, i.t.) produced profound motor ataxia in the rotarod test. Therefore, anti-allodynic effects of TAT-GESV cannot be attributed to nonspecific disruption of motor function. More work is necessary to demonstrate that nNOS-NOS1AP disruptors exhibit a better therapeutic ratio compared to NMDAR antagonists and nNOS inhibitors using small molecule inhibitors that, unlike TAT-GESV, can also be used systemically. Our findings collectively suggest that disruption of nNOS-NOS1AP protein-protein interactions represents a valuable therapeutic strategy for suppressing neuropathic pain without unwanted side effects associated with direct NMDAR-blockade (Figure 10). Our studies also demonstrate that nNOS-NOS1AP interface is a previously unrecognized target for the development of anti-allodynic agents to treat neuropathic pain.

## Acknowledgments

Supported by CA200417 (to AGH and MJC), DA037673 (to AGH and YYL) and NS078171 (to AH), the Indiana State Department of Health Spinal Cord Brain Injury Research grant ISDH/A70-2-079607 (to AH) and an Indiana University Collaborative Research Grant (to AGH, YYL and AH). The authors are grateful to Consulting Associate, David Endicott from Indiana Statistical Consulting Center for statistical advice.

## Abbreviations

<b>NMDAR</b>	<i>N</i> -methyl-D-aspartate receptor
<b>PSD95</b>	postsynaptic density 95kDa
<b>nNOS</b>	neuronal nitric oxide synthase
<b>NOS1AP</b>	nitric oxide synthase 1 adaptor protein
<b>PSNL</b>	partial sciatic nerve ligation
<b>p38 MAPK</b>	p38 mitogen-activated protein kinases
<b>p53</b>	tumor protein p53
<b>ERK1/2</b>	Extracellular signal-regulated kinases ½

## References

1. Aarts M, Liu Y, Liu L, Besshoh S, Arundine M, Gurd JW, Wang YT, Salter MW, Tymianski M. Treatment of ischemic brain damage by perturbing NMDA receptor- PSD-95 protein interactions. *Science*. 2002; 298(5594):846–850. [PubMed: 12399596]
2. Akimoto N, Honda K, Uta D, Beppu K, Ushijima Y, Matsuzaki Y, Nakashima S, Kido MA, Imoto K, Takano Y, Noda M. CCL-1 in the spinal cord contributes to neuropathic pain induced by nerve injury. *Cell Death Dis*. 2013; 4:e679. [PubMed: 23788036]
3. Ashpole NM, Hudmon A. Excitotoxic neuroprotection and vulnerability with CaMKII inhibition. *Molecular and cellular neurosciences*. 2011; 46(4):720–730. [PubMed: 21316454]

4. Boyette-Davis JA, Walters ET, Dougherty PM. Mechanisms involved in the development of chemotherapy-induced neuropathy. *Pain Manag.* 2015; 5(4):285–296. [PubMed: 26087973]
5. Bridges D, Thompson SW, Rice AS. Mechanisms of neuropathic pain. *British journal of anaesthesia.* 2001; 87(1):12–26. [PubMed: 11460801]
6. Candemir E, Kollert L, Weissflog L, Geis M, Muller A, Post AM, O’Leary A, Harro J, Reif A, Freudenberg F. Interaction of NOS1AP with the NOS-I PDZ domain: Implications for schizophrenia-related alterations in dendritic morphology. *Eur Neuropsychopharmacol.* 2016; 26(4): 741–755. [PubMed: 26861996]
7. Cao J, Viholainen JI, Dart C, Warwick HK, Leyland ML, Courtney MJ. The PSD95-nNOS interface: a target for inhibition of excitotoxic p38 stress-activated protein kinase activation and cell death. *The Journal of cell biology.* 2005; 168(1):117–126. [PubMed: 15631993]
8. Carey LM, Lee WH, Gutierrez T, Kulkarni PM, Thakur GA, Lai YY, Hohmann AG. Small molecule inhibitors of PSD95-nNOS protein-protein interactions suppress formalin-evoked Fos protein expression and nociceptive behavior in rats. *Neuroscience.* 2017
9. Courtney MJ, Li LL, Lai YY. Mechanisms of NOS1AP action on NMDA receptor-nNOS signaling. *Frontiers in cellular neuroscience.* 2014; 8:252. [PubMed: 25221472]
10. Coyle DE. Partial peripheral nerve injury leads to activation of astroglia and microglia which parallels the development of allodynic behavior. *Glia.* 1998; 23(1):75–83. [PubMed: 9562186]
11. Crown ED, Gwak YS, Ye Z, Johnson KM, Hulsebosch CE. Activation of p38 MAP kinase is involved in central neuropathic pain following spinal cord injury. *Experimental neurology.* 2008; 213(2):257–267. [PubMed: 18590729]
12. Cui H, Hayashi A, Sun HS, Belmares MP, Cobey C, Phan T, Schweizer J, Salter MW, Wang YT, Tasker RA, Garman D, Rabinowitz J, Lu PS, Tymianski M. PDZ protein interactions underlying NMDA receptor-mediated excitotoxicity and neuroprotection by PSD-95 inhibitors. *The Journal of neuroscience : the official journal of the Society for Neuroscience.* 2007; 27(37):9901–9915. [PubMed: 17855605]
13. D’Mello R, Marchand F, Pezet S, McMahon SB, Dickenson AH. Perturbing PSD-95 interactions with NR2B-subtype receptors attenuates spinal nociceptive plasticity and neuropathic pain. *Molecular therapy : the journal of the American Society of Gene Therapy.* 2011; 19(10):1780–1792. [PubMed: 21427709]
14. Deng L, Guindon J, Cornett BL, Makriyannis A, Mackie K, Hohmann AG. Chronic cannabinoid receptor 2 activation reverses paclitaxel neuropathy without tolerance or cannabinoid receptor 1-dependent withdrawal. *Biological psychiatry.* 2015; 77(5):475–487. [PubMed: 24853387]
15. Derijard B, Raingeaud J, Barrett T, Wu IH, Han J, Ulevitch RJ, Davis RJ. Independent human MAP-kinase signal transduction pathways defined by MEK and MKK isoforms. *Science.* 1995; 267(5198):682–685. [PubMed: 7839144]
16. Fairbanks CA. Spinal delivery of analgesics in experimental models of pain and analgesia. *Adv Drug Deliv Rev.* 2003; 55(8):1007–1041. [PubMed: 12935942]
17. Florio SK, Loh C, Huang SM, Iwamaye AE, Kitto KF, Fowler KW, Treiberg JA, Hayflick JS, Walker JM, Fairbanks CA, Lai Y. Disruption of nNOS-PSD95 protein-protein interaction inhibits acute thermal hyperalgesia and chronic mechanical allodynia in rodents. *British journal of pharmacology.* 2009; 158(2):494–506. [PubMed: 19732061]
18. Guindon J, Lai Y, Takacs SM, Bradshaw HB, Hohmann AG. Alterations in endocannabinoid tone following chemotherapy-induced peripheral neuropathy: effects of endocannabinoid deactivation inhibitors targeting fatty-acid amide hydrolase and monoacylglycerol lipase in comparison to reference analgesics following cisplatin treatment. *Pharmacological research : the official journal of the Italian Pharmacological Society.* 2013; 67(1):94–109.
19. Han Y, Smith MT. Pathobiology of cancer chemotherapy-induced peripheral neuropathy (CIPN). *Front Pharmacol.* 2013; 4:156. [PubMed: 24385965]
20. Hill MD, Martin RH, Mikulis D, Wong JH, Silver FL, Terbrugge KG, Milot G, Clark WM, Macdonald RL, Kelly ME, Boulton M, Fleetwood I, McDougall C, Gunnarsson T, Chow M, Lum C, Dodd R, Poublanc J, Krings T, Demchuk AM, Goyal M, Anderson R, Bishop J, Garman D, Tymianski M. investigators Et. Safety and efficacy of NA-1 in patients with iatrogenic stroke after

- endovascular aneurysm repair (ENACT): a phase 2, randomised, double-blind, placebo-controlled trial. *Lancet Neurol.* 2012; 11(11):942–950. [PubMed: 23051991]
21. Hudmon A, Lebel E, Roy H, Sik A, Schulman H, Waxham MN, De Koninck P. A mechanism for Ca<sup>2+</sup>/calmodulin-dependent protein kinase II clustering at synaptic and nonsynaptic sites based on self-association. *The Journal of neuroscience : the official journal of the Society for Neuroscience.* 2005; 25(30):6971–6983. [PubMed: 16049173]
  22. Hylden JL, Wilcox GL. Intrathecal morphine in mice: a new technique. *European journal of pharmacology.* 1980; 67(2–3):313–316. [PubMed: 6893963]
  23. Ishii H, Shibuya K, Ohta Y, Mukai H, Uchino S, Takata N, Rose JA, Kawato S. Enhancement of nitric oxide production by association of nitric oxide synthase with N-methyl-D-aspartate receptors via postsynaptic density 95 in genetically engineered Chinese hamster ovary cells: real-time fluorescence imaging using nitric oxide sensitive dye. *J Neurochem.* 2006; 96(6):1531–1539. [PubMed: 16464237]
  24. Jaffrey SR, Snowman AM, Eliasson MJ, Cohen NA, Snyder SH. CAPON: a protein associated with neuronal nitric oxide synthase that regulates its interactions with PSD95. *Neuron.* 1998; 20(1):115–124. [PubMed: 9459447]
  25. Ji RR, Gereau RWt, Malcangio M, Strichartz GR. MAP kinase and pain. *Brain Res Rev.* 2009; 60(1):135–148. [PubMed: 19150373]
  26. Ji RR, Suter MR. p38 MAPK, microglial signaling, and neuropathic pain. *Molecular pain.* 2007; 3:33. [PubMed: 17974036]
  27. Lee WH, Xu Z, Ashpole NM, Hudmon A, Kulkarni PM, Thakur GA, Lai YY, Hohmann AG. Small molecule inhibitors of PSD95-nNOS protein-protein interactions as novel analgesics. *Neuropharmacology.* 2015; 97:464–475. [PubMed: 26071110]
  28. Li LL, Cisek K, Courtney MJ. Efficient Binding of the NOS1AP C-Terminus to the nNOS PDZ Pocket Requires the Concerted Action of the PDZ Ligand Motif, the Internal ExF Site and Structural Integrity of an Independent Element. *Front Mol Neurosci.* 2017; 10:58. [PubMed: 28360833]
  29. Li LL, Ginet V, Liu X, Vergun O, Tuittila M, Mathieu M, Bonny C, Puyal J, Truttmann AC, Courtney MJ. The nNOS-p38MAPK pathway is mediated by NOS1AP during neuronal death. *The Journal of neuroscience : the official journal of the Society for Neuroscience.* 2013; 33(19):8185–8201. [PubMed: 23658158]
  30. Li LL, Melero-Fernandez de Mera RM, Chen J, Ba W, Kasri NN, Zhang M, Courtney MJ. Unexpected Heterodivalent Recruitment of NOS1AP to nNOS Reveals Multiple Sites for Pharmacological Intervention in Neuronal Disease Models. *The Journal of neuroscience : the official journal of the Society for Neuroscience.* 2015; 35(19):7349–7364. [PubMed: 25972165]
  31. Lin X, Wang M, Zhang J, Xu R. p38 MAPK: a potential target of chronic pain. *Curr Med Chem.* 2014; 21(38):4405–4418. [PubMed: 25245374]
  32. Ma W, Quirion R. Partial sciatic nerve ligation induces increase in the phosphorylation of extracellular signal-regulated kinase (ERK) and c-Jun N-terminal kinase (JNK) in astrocytes in the lumbar spinal dorsal horn and the gracile nucleus. *Pain.* 2002; 99(1–2):175–184. [PubMed: 12237195]
  33. Matsumoto M, Xie W, Ma L, Ueda H. Pharmacological switch in Abeta-fiber stimulation-induced spinal transmission in mice with partial sciatic nerve injury. *Molecular pain.* 2008; 4:25. [PubMed: 18620588]
  34. Mo SF, Liao GY, Yang J, Wang MY, Hu Y, Lian GN, Kong LD, Zhao Y. Protection of neuronal cells from excitotoxicity by disrupting nNOS-PSD95 interaction with a small molecule SCR-4026. *Brain research.* 2016; 1648(Pt A):250–256. [PubMed: 27421179]
  35. Motulsky H. *Intuitive Biostatistics: A Nonmathematical Guide to Statistical Thinking.* 3. Oxford University Press; 2013.
  36. Nikam SS, Meltzer LT. NR2B selective NMDA receptor antagonists. *Curr Pharm Des.* 2002; 8(10):845–855. [PubMed: 11945135]
  37. Persons DL, Yazlovitskaya EM, Pelling JC. Effect of extracellular signal-regulated kinase on p53 accumulation in response to cisplatin. *The Journal of biological chemistry.* 2000; 275(46):35778–35785. [PubMed: 10958792]

38. Raingeaud J, Whitmarsh AJ, Barrett T, Derijard B, Davis RJ. MKK3- and MKK6-regulated gene expression is mediated by the p38 mitogen-activated protein kinase signal transduction pathway. *Mol Cell Biol*. 1996; 16(3):1247–1255. [PubMed: 8622669]
39. Sattler R, Xiong Z, Lu WY, Hafner M, MacDonald JF, Tymianski M. Specific coupling of NMDA receptor activation to nitric oxide neurotoxicity by PSD-95 protein. *Science*. 1999; 284(5421): 1845–1848. [PubMed: 10364559]
40. Schepens J, Cuppen E, Wieringa B, Hendriks W. The neuronal nitric oxide synthase PDZ motif binds to -G(D,E)XV\* carboxyterminal sequences. *FEBS Lett*. 1997; 409(1):53–56. [PubMed: 9199503]
41. She QB, Chen N, Dong Z. ERKs and p38 kinase phosphorylate p53 protein at serine 15 in response to UV radiation. *The Journal of biological chemistry*. 2000; 275(27):20444–20449. [PubMed: 10781582]
42. Sisignano M, Baron R, Scholich K, Geisslinger G. Mechanism-based treatment for chemotherapy-induced peripheral neuropathic pain. *Nat Rev Neurol*. 2014; 10(12):694–707. [PubMed: 25366108]
43. Slivicki RA, Xu Z, Kulkarni PM, Pertwee RG, Mackie K, Thakur GA, Hohmann AG. Positive allosteric modulation of CB1 suppresses pathological pain without producing tolerance or dependence. *Biological psychiatry*. 2017 In Press.
44. Smith AE, Xu Z, Lai YY, Kulkarni PM, Thakur GA, Hohmann AG, Crystal JD. Source memory in rats is impaired by an NMDA receptor antagonist but not by PSD95-nNOS protein-protein interaction inhibitors. *Behav Brain Res*. 2016; 305:23–29. [PubMed: 26909849]
45. Svensson CI, Hua XY, Protter AA, Powell HC, Yaksh TL. Spinal p38 MAP kinase is necessary for NMDA-induced spinal PGE(2) release and thermal hyperalgesia. *Neuroreport*. 2003; 14(8):1153–1157. [PubMed: 12821799]
46. Svensson CI, Marsala M, Westerlund A, Calcutt NA, Campana WM, Freshwater JD, Catalano R, Feng Y, Protter AA, Scott B, Yaksh TL. Activation of p38 mitogen-activated protein kinase in spinal microglia is a critical link in inflammation-induced spinal pain processing. *J Neurochem*. 2003; 86(6):1534–1544. [PubMed: 12950462]
47. Tochio H, Mok YK, Zhang Q, Kan HM, Brecht DS, Zhang M. Formation of nNOS/PSD-95 PDZ dimer requires a preformed beta-finger structure from the nNOS PDZ domain. *Journal of molecular biology*. 2000; 303(3):359–370. [PubMed: 11031113]
48. Tochio H, Zhang Q, Mandal P, Li M, Zhang M. Solution structure of the extended neuronal nitric oxide synthase PDZ domain complexed with an associated peptide. *Nat Struct Biol*. 1999; 6(5): 417–421. [PubMed: 10331866]
49. Wang J, Jin L, Zhu Y, Zhou X, Yu R, Gao S. Research progress in NOS1AP in neurological and psychiatric diseases. *Brain research bulletin*. 2016; 125:99–105. [PubMed: 27237129]
50. Wang P, Zhang Q, Tochio H, Fan JS, Zhang M. Formation of a native-like beta-hairpin finger structure of a peptide from the extended PDZ domain of neuronal nitric oxide synthase in aqueous solution. *European journal of biochemistry / FEBS*. 2000; 267(11):3116–3122.
51. Ward SJ, Ramirez MD, Neelakantan H, Walker EA. Cannabidiol prevents the development of cold and mechanical allodynia in paclitaxel-treated female C57B16 mice. *Anesthesia and analgesia*. 2011; 113(4):947–950. [PubMed: 21737705]
52. Xu M, Bruchas MR, Ippolito DL, Gendron L, Chavkin C. Sciatic nerve ligation-induced proliferation of spinal cord astrocytes is mediated by kappa opioid activation of p38 mitogen-activated protein kinase. *The Journal of neuroscience : the official journal of the Society for Neuroscience*. 2007; 27(10):2570–2581. [PubMed: 17344394]
53. Zhang H, Yoon SY, Zhang H, Dougherty PM. Evidence that spinal astrocytes but not microglia contribute to the pathogenesis of Paclitaxel-induced painful neuropathy. *The journal of pain : official journal of the American Pain Society*. 2012; 13(3):293–303. [PubMed: 22285612]
54. Zheng FY, Xiao WH, Bennett GJ. The response of spinal microglia to chemotherapy-evoked painful peripheral neuropathies is distinct from that evoked by traumatic nerve injuries. *Neuroscience*. 2011; 176:447–454. [PubMed: 21195745]

55. Zhou HY, Chen SR, Pan HL. Targeting N-methyl-D-aspartate receptors for treatment of neuropathic pain. *Expert review of clinical pharmacology*. 2011; 4(3):379–388. [PubMed: 21686074]
56. Zhou L, Li F, Xu HB, Luo CX, Wu HY, Zhu MM, Lu W, Ji X, Zhou QG, Zhu DY. Treatment of cerebral ischemia by disrupting ischemia-induced interaction of nNOS with PSD-95. *Nature medicine*. 2010; 16(12):1439–1443.
57. Zhu LJ, Li TY, Luo CX, Jiang N, Chang L, Lin YH, Zhou HH, Chen C, Zhang Y, Lu W, Gao LY, Ma Y, Zhou QG, Hu Q, Hu XL, Zhang J, Wu HY, Zhu DY. CAPON-nNOS coupling can serve as a target for developing new anxiolytics. *Nature medicine*. 2014; 20(9):1050–1054.
58. Zhuang ZY, Kawasaki Y, Tan PH, Wen YR, Huang J, Ji RR. Role of the CX3CR1/p38 MAPK pathway in spinal microglia for the development of neuropathic pain following nerve injury-induced cleavage of fractalkine. *Brain Behav Immun*. 2007; 21(5):642–651. [PubMed: 17174525]

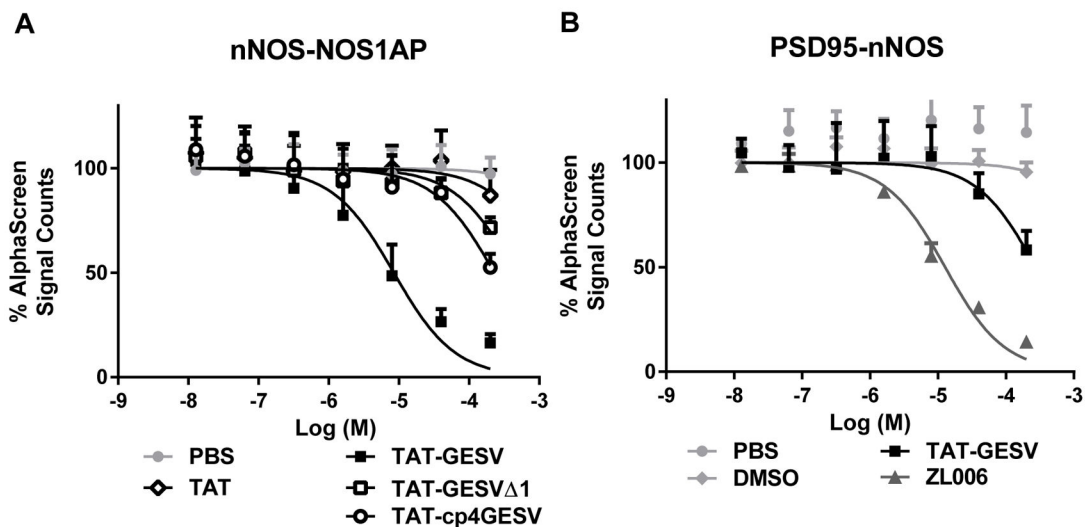


**Figure 1.**

TAT-GESV disrupts nNOS-NOS1AP but not PSD95-nNOS binding in AlphaScreen. **A.** TAT-GESV disrupted His-nNOS<sub>1-299</sub> and GST-NOS1AP<sub>400-506</sub> binding presented as % AlphaScreen Signal Counts with an IC<sub>50</sub> of 8.47  $\mu$ M. Neither TAT-GESV 1 nor TAT-cp4GESV disrupted the binding between these two proteins under analogous conditions (n = 4–9). **B.** TAT-GESV did not disrupt interactions between His-PSD95<sub>1-392</sub> and GST-nNOS<sub>1-299</sub> under conditions in which the small molecule PSD95-nNOS inhibitor ZL006 reliably disrupted this binding with an IC<sub>50</sub> of 12.76  $\mu$ M. Data are Mean  $\pm$  S.D.

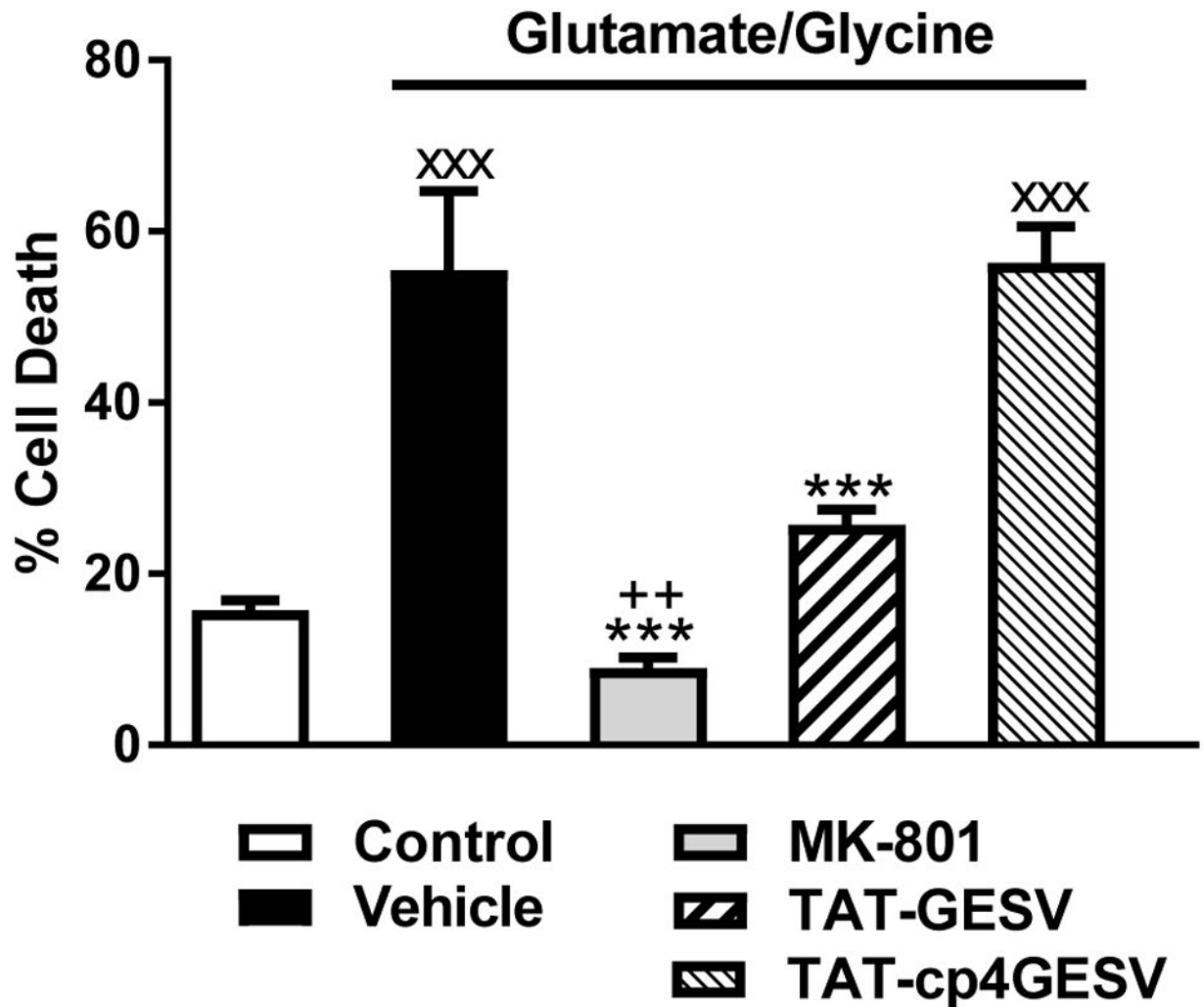


**Figure 2.**

The active but not the inactive nNOS-NOS1AP disruptor inhibits glutamate-induced cell death. Pretreatment with the active peptide TAT-GESV (10  $\mu$ M) or the NMDAR antagonist MK-801 (20  $\mu$ M) protected against cell death induced by glutamate (100  $\mu$ M)/glycine (10  $\mu$ M) in primary cortical neurons relative to vehicle pre-treatment. Cell death was lower following pre-treatment with the active nNOS-NOS1AP disruptor TAT-GESV compared to the inactive peptide TAT-cp4GESV (10  $\mu$ M) (see Figure 1 for binding data in AlphaScreen), and failed to protect against glutamate/glycine-induced cell death ( $n = 3-4$ ). \*\*\* $p < 0.001$  vs. vehicle and TAT-cp4GESV; <sup>xxx</sup> $p < 0.001$  vs. all groups except vehicle or TAT-cp4GESV; ++ $p < 0.01$  vs. TAT-GESV (One-way ANOVA followed by Bonferroni's *post hoc* test). Data are Mean  $\pm$  S.D.



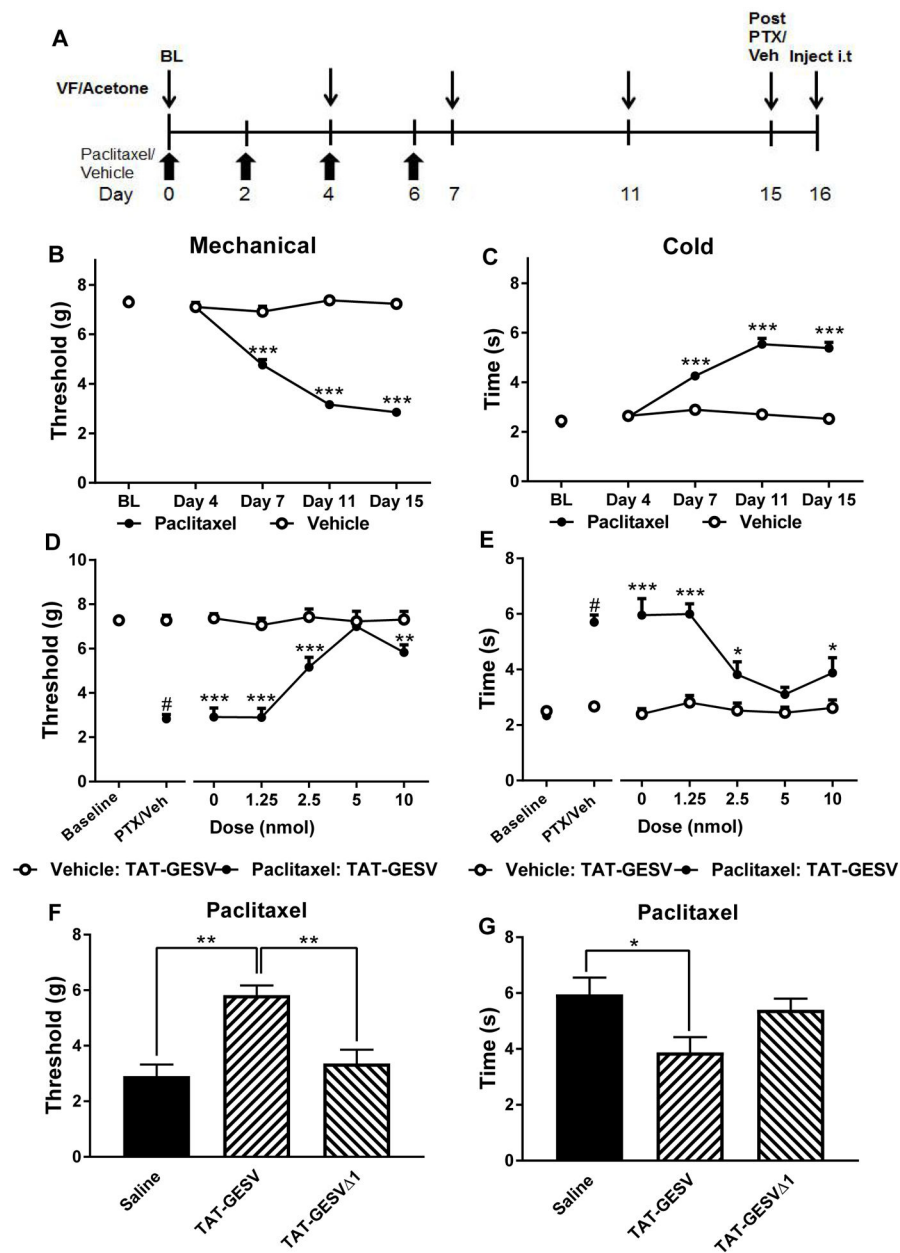


**Figure 3.** TAT-GESV, a peptide inhibitor of nNOS-NOS1AP interactions, suppressed paclitaxel-induced mechanical and cold allodynia. **A**. Dosing and testing scheme used to evaluate the anti-allodynic efficacy of the nNOS-NOS1AP inhibitor in the paclitaxel model. Paw withdrawal threshold (g) was measured using an electronic von Frey anesthesiometer to assess mechanical sensitivity and duration (sec) of responding to acetone stimulation of the hindpaw was measured to assess cold sensitivity. Behavioral testing of mechanical and cold sensitivity was performed at time points shown by the thin arrows. Paclitaxel or vehicle was administered i.p. at time points indicated by the bold arrows. **B**, **C**. Paclitaxel lowered (B) mechanical paw withdrawal thresholds and increased (C) duration of cold responding

relative to cremophor-vehicle treatment in a time-dependent manner. Behavioral hypersensitivities were present beginning on day 7 and were ongoing throughout the observation interval. \*\*\* $p < 0.0001$  from Day 7–15 (Two-way repeated measures ANOVA followed by Bonferroni's *post hoc* test). **D, E.** TAT-GESV dose-dependently (D) increased mechanical paw withdrawal thresholds and (E) reduced cold response times in paclitaxel-treated mice. # $p < 0.001$  (paired sample t-test vs. baseline). \* $p < 0.05$ ; \*\* $p < 0.01$ ; \*\*\* $p < 0.001$  vs. corresponding vehicle: TAT-GESV group (Two-way ANOVA followed by Bonferroni's *post hoc* test). The 5 nmol dose of TAT-GESV normalized responding to levels observed in mice receiving vehicle in lieu of paclitaxel. **F, G.** In paclitaxel-treated mice, TAT-GESV (10 nmol, i.t.) increased (F) mechanical paw withdrawal thresholds relative to both saline (i.t.) and TAT-GESV 1 (10 nmol, i.t.) treatment and lowered (G) cold response duration relative to saline (i.t.) treatment. \* $p < 0.05$ ; \*\* $p < 0.01$  (One-way ANOVA followed by Bonferroni's *post hoc* test). Data are Mean  $\pm$  S.E.M. (n = 6 per group).

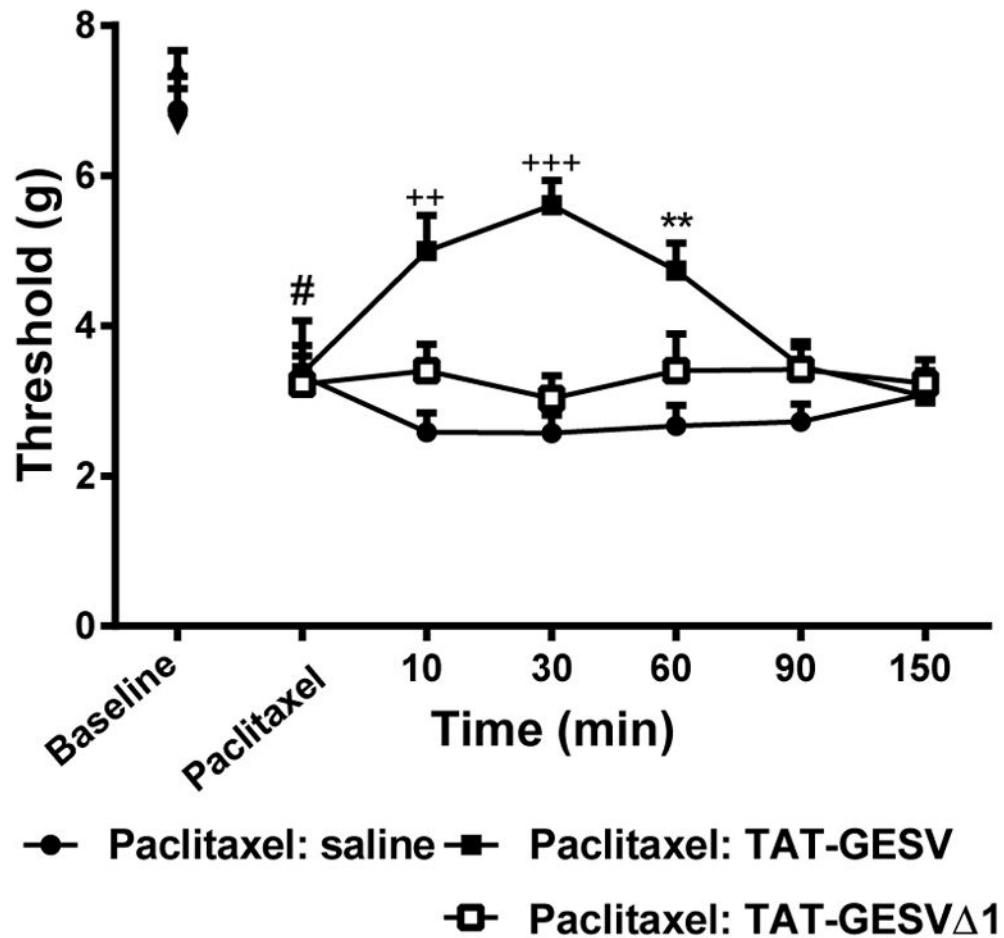


**Figure 4.** Duration of action of TAT-GESV-induced suppression of paclitaxel-induced mechanical allodynia. TAT-GESV (5 nmol i.t.) increased mechanical paw withdrawal thresholds relative to either saline (i.t.) or TAT-GESV 1 (5 nmol i.t.) treatment across the observation interval ( $p < 0.01$  for each comparison). Anti-allodynic effects of TAT-GESV in paclitaxel-treated mice were time-dependent. \*\* $p < 0.01$  vs. saline; ++ $p < 0.01$ ; +++ $p < 0.001$  vs. saline and TAT-GESV 1; # $p < 0.01$  vs. baseline for all groups (Two-way repeated measures ANOVA followed by Bonferroni's *post hoc* test). Data are Mean  $\pm$  S.E.M. ( $n = 5$  per group).

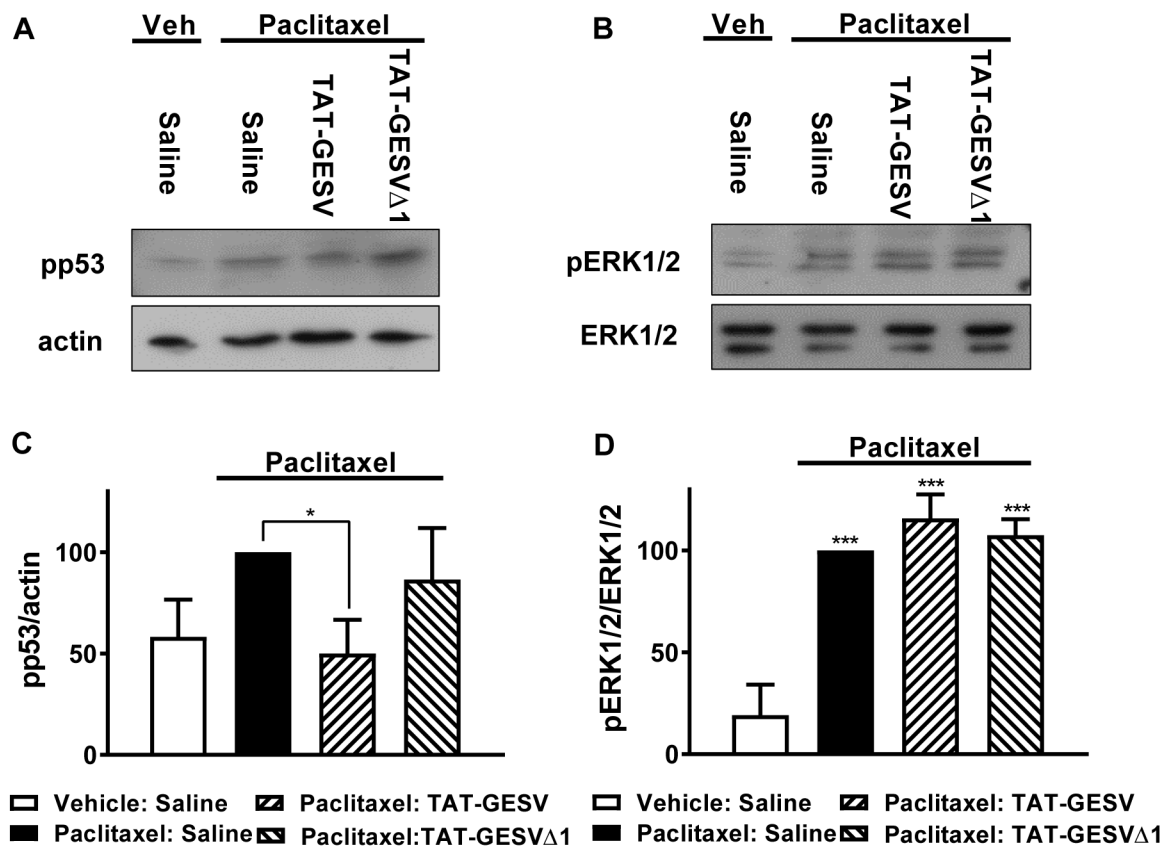


**Figure 5.**

Intrathecal administration of TAT-GESV reduced phosphorylation of Ser15-p53 (pp53) levels induced by paclitaxel injection independent of the ERK1/2 pathway. **A**. In lumbar spinal cords derived from paclitaxel-treated mice, TAT-GESV (5 nmol, i.t.) reduced (**A**, **C**) p53 activation relative to saline (i.t.) but not TAT-GESV  $\Delta$ 1 (5 nmol, i.t.) (\*p < 0.05 vs. saline; One way ANOVA followed by Bonferroni's multiple comparison test). **B**, **D**. pERK1/2 was elevated in lumbar spinal cord derived from all paclitaxel-treated groups, but ERK1/2 activation was not blocked by TAT-GESV (i.t.). \*\*\*p < 0.001 vs. Vehicle: Saline (One-way ANOVA followed by Bonferroni's *post hoc* test). Data are Mean  $\pm$  S.E.M. (n = 5 per group).

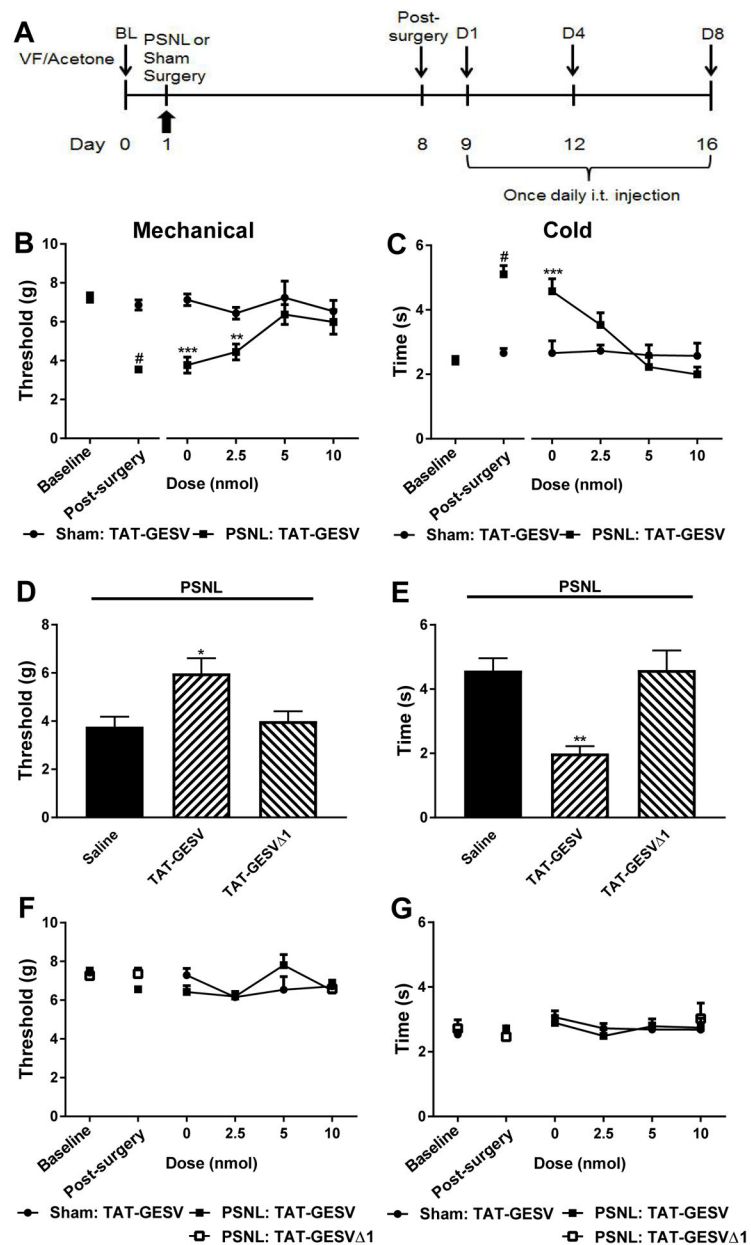


**Figure 6.** Intrathecal administration of TAT-GESV, a peptide inhibitor of nNOS-NOS1AP, suppressed PSNL-induced mechanical and cold allodynia without affecting responses in the contralateral paw or in sham-operated mice. **A**. Surgery and testing scheme used to evaluate the anti-allodynic efficacy of nNOS-NOS1AP inhibitor in the PSNL model. Paw withdrawal threshold (g) was measured using an electronic von Frey anesthesiometer to assess mechanical sensitivity and duration (sec) of responding to acetone stimulation of the hindpaw was measured to assess cold sensitivity. Behavioral testing of mechanical and cold sensitivity was performed at time points shown by the thin arrows. PSNL or sham surgery was performed at time point indicated with the bold arrow. **B, C**. Mechanical (**B**) and cold (**C**) allodynia evoked by PSNL was dose-dependently suppressed by TAT-GESV. TAT-GESV

(5 and 10 nmol i.t.) normalized responding to levels observed in sham-operated mice receiving the same doses. # $p < 0.001$  vs. baseline (Paired sample t-test). \*\* $p < 0.01$ ; \*\*\* $p < 0.001$  vs. corresponding sham-operated group (Two-way ANOVA followed by Bonferroni's *post hoc* test). **D, E.** In the paw ipsilateral to PSNL, TAT-GESV (10 nmol, i.t.) (D) increased mechanical paw withdrawal thresholds and (E) reduced duration of cold responding relative to either saline (i.t.) or TAT-GESV 1 (10 nmol, i.t.) treatment. \* $p < 0.05$ , \*\* $p < 0.01$  vs. saline and TAT-GESV 1 (One-way ANOVA followed by Bonferroni's *post hoc* test). **F, G.** TAT-GESV did not alter (F) mechanical paw withdrawal thresholds or (G) cold response time in the paw contralateral to PSNL or sham surgery (Two-way ANOVA). Data are Mean  $\pm$  S.E.M. (n = 6–10 per group).

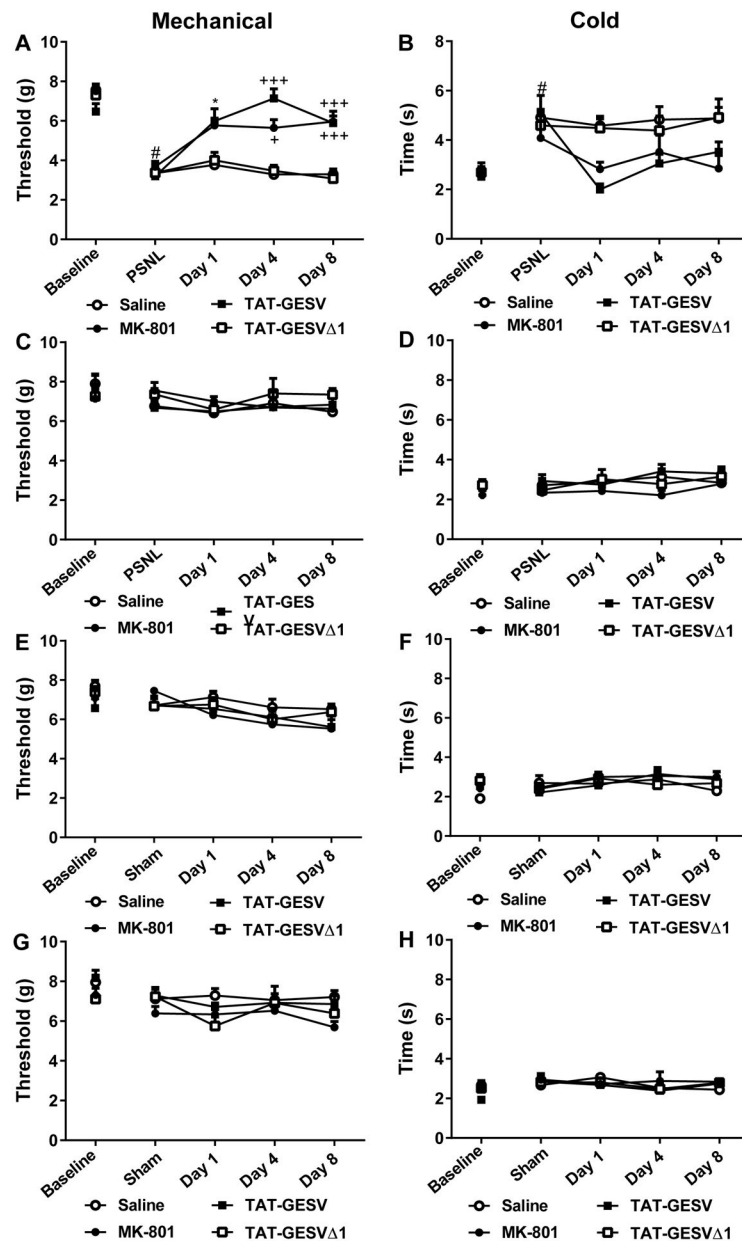


**Figure 7.**

Repeated intrathecal dosing with the nNOS-NOS1AP inhibitor TAT-GESV (10 nmol, i.t.) suppressed PSNL-induced mechanical and cold allodynia without altering responses in the contralateral paw or in sham-operated mice. **A, B.** In mice subjected to PSNL, repeated once daily intrathecal injection of TAT-GESV (10 nmol i.t.) and MK-801 (5 nmol i.t.) across eight consecutive days elevated (A) mechanical paw withdrawal thresholds relative to saline and TAT-GESV 1 throughout the observation interval ( $p < 0.0001$  for each comparison; Two-way repeated measures ANOVA followed by Bonferroni's *post hoc* test). Suppression of mechanical allodynia induced by TAT-GESV and MK-801 was also time-dependent. Repeated intrathecal injection of TAT-GESV reduced (B) duration of cold responses relative to saline ( $p < 0.0001$ ) throughout the observation interval. Effects of TAT-GESV on PSNL-

induced mechanical and cold allodynia were similar to MK-801. # $p < 0.05$  vs. baseline; \* $p < 0.05$  vs. saline; +++ $p < 0.001$  vs. saline and TAT-GESV 1 (Two-way repeated measures ANOVA followed by Bonferroni's *post hoc* test). **C, D.** TAT-GESV did not alter (C) mechanical paw withdrawal thresholds or (D) cold response time in the paw contralateral to PSNL. **E–H.** TAT-GESV did not alter responsiveness to mechanical or cold stimulation in either the (E,F) ipsilateral or (G,H) contralateral paw of sham-operated mice. A–H. Data was analyzed by Two-way repeated measures ANOVA followed by Bonferroni *post hoc* test. Data are Mean  $\pm$  S.E.M. (n = 5–10 per group).



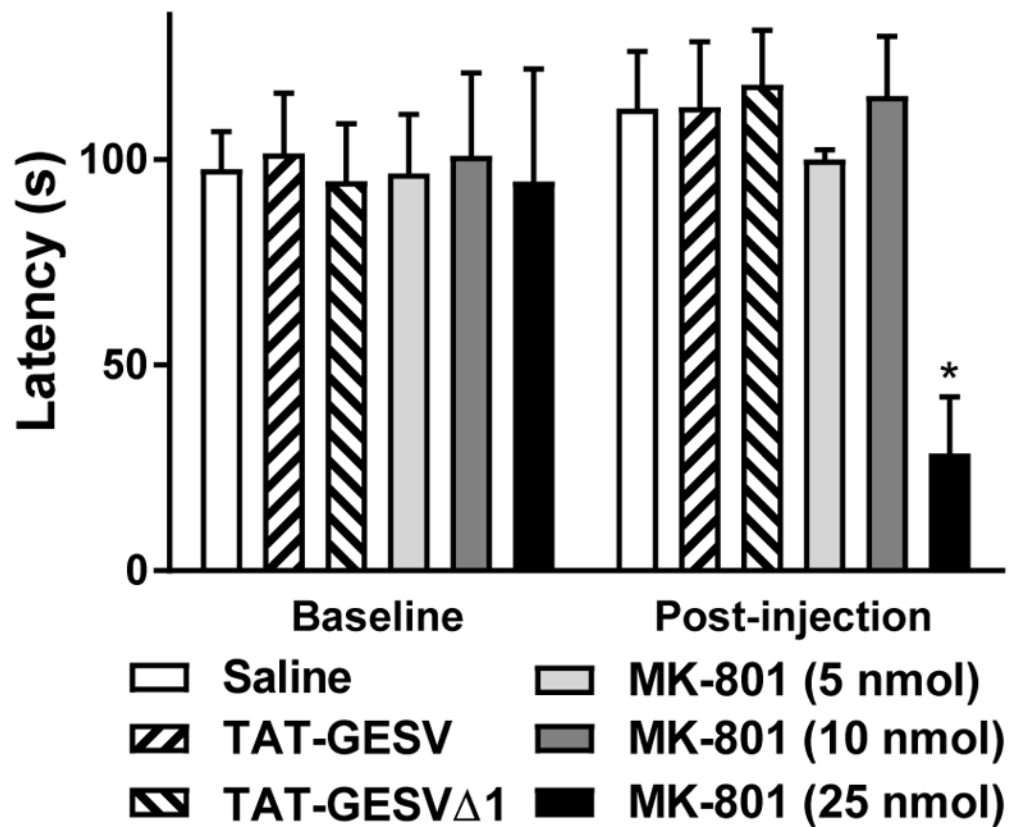


**Figure 8.**

Intrathecal injection of MK-801 (25 nmol, i.t.) but not TAT-GESV (10 nmol, i.t.) or TAT-GESV $\Delta$ 1 (10 nmol, i.t.) produced motor ataxia in the rota-rod test. MK-801 (25 nmol i.t.) reduced post-injection rota-rod descent latency relative to all other intrathecal treatments. \* $p < 0.05$  vs. all post-injection groups (Two-way repeated measures ANOVA followed by Bonferroni's *post hoc* test). Data are Mean  $\pm$  S.E.M. (n= 4–8 per group).

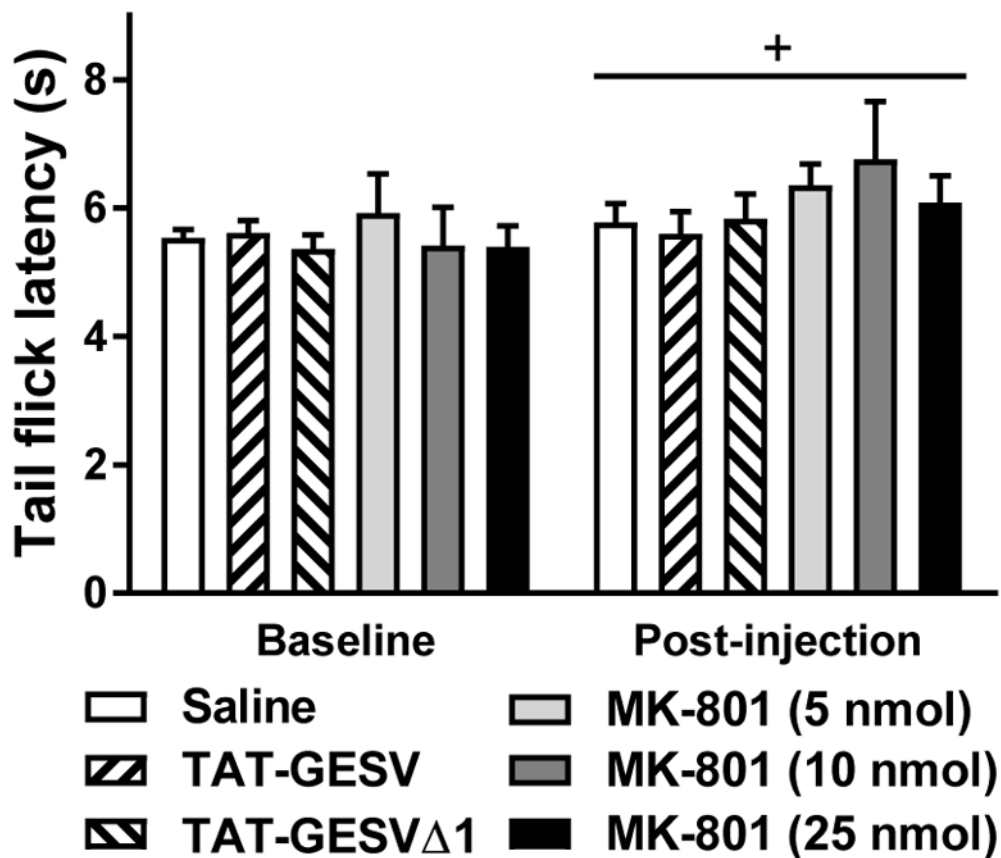


**Figure 9.** TAT-GESV at the highest dose assessed (10 nmol i.t.) did not produce antinociception or heat hypersensitivity in a radiant-heat tail flick test. Similar results were observed with MK-801 (5, 10 and 25 nmol i.t.). Post-injection tail-flick latencies differed from pre-injection tail-flick latencies but this effect was not dependent upon intrathecal treatment. + $p < 0.05$  (Two-way repeated measures ANOVA). Data are Mean  $\pm$  S.E.M. ( $n = 6-8$  per group).

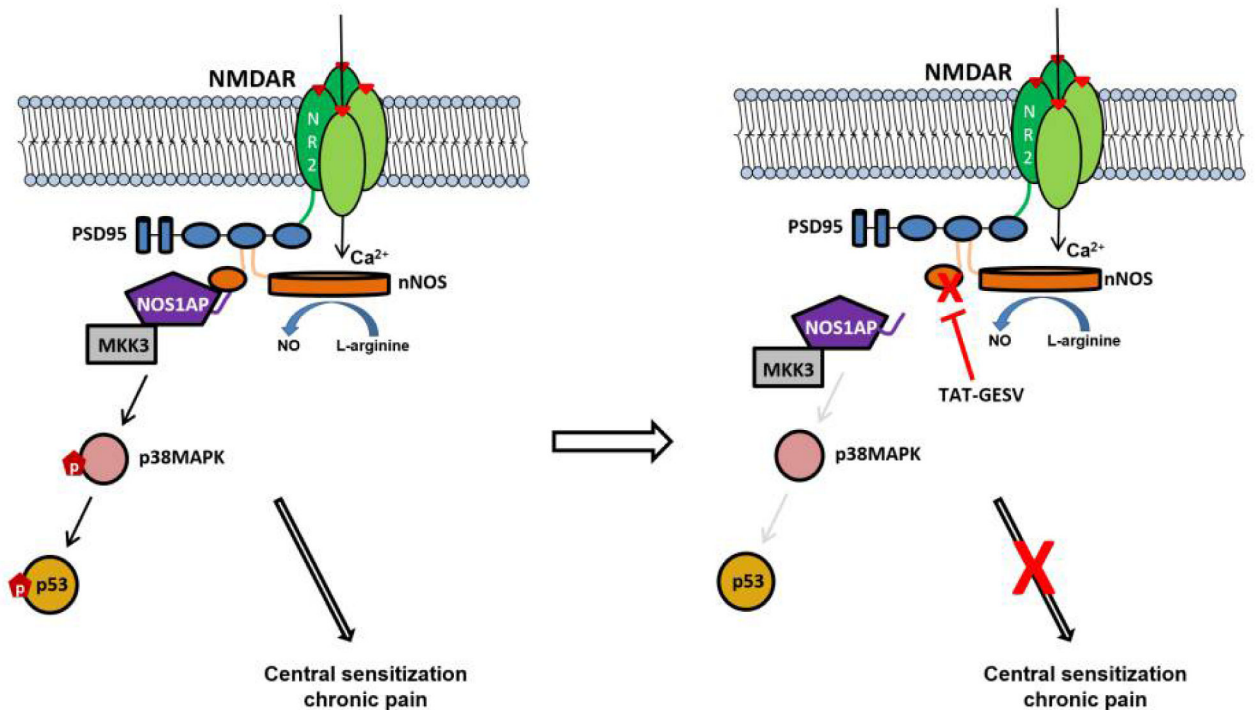


**Figure 10.**

Model depicting the proposed effect of the membrane-permeant peptide TAT-GESV on NMDAR signaling in neuropathic pain. NMDARs typically consist of two NR1 subunits and two NR2 subunits. The latter can interact via its C-terminus with the PDZ1 domain of the scaffolding protein postsynaptic density 95 kDa (PSD95), which tethers the enzyme neuronal nitric oxide synthase (nNOS) to the NMDAR, whereas the PDZ2 domain of PSD95 is free to recruit nNOS via its  $\beta$ -finger (orange loop). Preceding the  $\beta$ -finger of nNOS is a canonical PDZ domain that recruits NOS1AP, an adaptor protein that recruits the p38 MAPK activator MKK3 and mediates nNOS-dependent activation of p38MAPK activity [29] (left panel). Activation of p38 MAPK leads to phosphorylation of its substrates such as serine 15 on p53, which in this study is used as a surrogate marker of p38 MAPK activation. We propose that this pathway mediates the contribution of NMDAR-nNOS signaling to central sensitization and chronic pain. We postulate that TAT-GESV (right panel) displaces NOS1AP from the PDZ domain of nNOS, uncoupling the p38 MAPK-p53 pathway from the NMDAR-PSD95-nNOS complex, thereby reducing central sensitization and chronic pain.